JOM
https://doi.org/10.1007/s11837-026-08273-x

Materials Engineering of Elastomer–Metal Interfaces Under Corrosion, Wear, and Adhesion Stressors

S. BHUVANESH,[1] V. PRAKASH,[1] V. ARUL,[2] P. SARAVANAN,[3] N. SUBASREE,[4] K. RADHAKRISHNAN,[1,9] R. SURIYAPRAKASH,[5] MOHAMMED ALSAWAT,[6] M. SHERLIN NIVETHA,[7] and JOTHI VINOTH KUMAR[8,10]

1.—Department of Chemistry, Centre for Material Chemistry, Karpagam Academy of Higher Education, Coimbatore, Tamil Nadu 641021, India. 2.—Department of Chemistry, Sri Eshwar College of Engineering (Autonomous), Coimbatore, Tamil Nadu 641202, India. 3.—Department of Chemistry, St. Joseph's College of Engineering, OMR, Chennai, Tamil Nadu 600119, India. 4.—Department of Chemistry, School of Basic Science, Vels Institute of Science, Technology and Advanced Studies (VISTAS), Pallavaram, Chennai, Tamilnadu 600117, India. 5.—Centre for Research in Environment, Sustainability Advocacy and Climate Change (REACH), Directorate of Research, SRM Institute of Science and Technology, Kattankulathur, Chengalpattu District Tamil Nadu, India. 6.—Department of Chemistry, College of Science, Taif University, Taif, Saudi Arabia. 7.—Department of Chemistry, Sathyabama Institute of Science and Technology (Deemed to be University), Vadamangalam, Sriperumbudur, Tamil Nadu 02108, India. 8.—Centre for Applied Nanomaterials, Chennai Institute of Technology, Chennai 600069, India. 9.—e-mail: raddhakrishnan21@gmail.com. 10.—e-mail: drjvinoth@gmail.com

Elastomer–metal interfaces find applications in the automotive, aerospace, and biomedical industries, and are affected by environmental degradation, which is mainly corrosion, wear, and adhesion failure. Harsh service conditions, such as wet conditions, changes in temperatures, chemicals, mechanical forces contribute to the interfacial weakening process due to electrochemical reactions, crack propagation, and delamination, eventually cause a failure of the system. This review highlights the fundamental pathways of interfacial degradation and the interaction effect that occur between chemical, mechanical, and environmental stressors. An integrated system of chemo-mechanical–environmental degradation is considered, whereby corrosion, wear, loss of adhesion, and mechanical fatigue are not considered independent processes but rather they interact. This model emphasizes the acceleration of other stressors, which is caused by the damage of one stressor and by the feedback of other stressors at the elastomer–metal interface. The methods of mitigation are discussed, as well as surface treatment, incorporation of nanoparticles to strengthen the composite, the application of special adhesives, and bioinspired alternatives, such as sacrificial bonding and self-healing. Recent development of multifunctional elastomer–metal composites exhibit toughness and damping, corrosion resistance, and bond durability. Other issues highlight the importance of additional studies to solve the complexity of synergistic degradation in real-life scenarios. Smart coatings, predictive modeling, and resilient, sustainable, and adaptive materials are some of the future opportunities.

INTRODUCTION

Nature has the prototype of materials which have tribologically and environmentally resilient designs. The hierarchical microstructuring of the biological microstructures of the bio-inspired teeth, nails, and

(Received December 4, 2025; accepted March 2, 2026)

Published online: 03 April 2026

soft pads is designed to optimize wear resistance, flexibility, and energy absorption, and to reduce weight, which allows repetitive loading. The phenomenon of nature is that stiffness and toughness are balanced to increase the contact duration between two metals, and man has employed rigid materials; therefore, material selection and microstructural design play a vital role in reducing the impact of environmental degradation and tribological wear.[1] The severe conditions that are experienced in the industry when dealing with elastomer–metal interfaces are harsh chemical and mechanical. Seals and packers are exposed to pressure, temperature, and abrasive fluids in the oil and gas industry which contribute 31% and 21% of the overall global oil and gas production, respectively. Polymer structure, crystallinity, cross-link density, and elastomer–fluid polarity, which are determined to a large extent by the solubility parameters (δ), are the factors that determine failures, such as seal hardening, swelling, chemical attack, and fragmentation.[2]

Bio-based alternatives made of cellulose, lignin, and oleaginous (plant-based) have a more reasonable sustainability or performance trade-off. Interventions to overcome these failures are strain-induced crystallization, hierarchical hydrogen bonding, and dynamic hard domains, which will guarantee that increased durability does not lead to reduced end-of-life recyclability.[3] The application of polydimethylsiloxane (PDMS) is extensive because of its malleability, spotting, and biocompatibility, although oxygen and moisture can flow through the polymers and corrode the metal films laid by plasma oxidation or physical vapor deposition. Integrated concepts, such as moisture-impermeable network elastomer (MINE), involve the utilization of PDMS and elastomers of low permeability, including IIR, which are necessary to address the impact of moisture-induced degradation without compromising stretchiness.[4] The appearance of new types of degradable and self-healing elastomers also extend the life of devices and decrease the waste. Polyurethane is made of reversible cross-linked networks that are based on lignin and has a tensile strength (2.72 MPa), elongation (712%), self-healing properties, and degradability, which allows its use in stretchable substrates.[5] Hydraulic and reciprocating seals have been life-tested in service to investigate their tribological performance, which is reminiscent of the significance of the accelerated life testing which scaled the number of adhesive wear test coupons completed between 2008 and 2018 in many other published literature studies on hydraulic seals and reciprocating seal service.[6] The copper employed in biomedical devices is tough even at fatigue, but porous structures may cause weakening of materials under the effect of stress concentration.[7]

Permittivity and electromechanical coupling is increased by elastomer–metal composites (e.g., liquid metal-embedded elastomers), but the dielectric breakdown strength decreases due to the presence of very large metal droplets. The submicron inclusions are not so degrading to the durability.[8] Hierarchically or re-entrant-structured non-frictional elastomeric surfaces are superhydrophobic and self-healing, but also weak. UV-responsive self-healing elastomer–metal surfaces[9] are tough and self-healing, and the wettability of the sample is dynamically controllable on top of sacrificial aluminum templates that are further improved with titania through atomic layer deposition (ALD). There are also improvements in elastomer blending and compatibility to improve the performance of the elastomers with metals. Thermoplastic poly(ether–ester) elastomers also have mixtures of hard domains and soft elastic blocks and are also oil- and abrasion-resistant in their use as automotive seals.[10] Another dominant cause of swelling, shrinkage, and chemical degradation is the effect of elastomer–fluid interactions which are controlled by the terms of polarity, crystallinity, and the density of cross-links.[2] Interfaces preferred in corrosion resistance are widened by the development of ionic conducting elastomers and biodegradable 2-pyrone-4,6-dicarboxylic acids, the expanded polytetrafluoroethylene (ePTFE) grafts that are coated with poly(1,8-octanediol citrate) are hemocompatible, and the ePTFE materials have desired combined properties, as envisioned by CsE, of stretchability, transparency, and temperature resistance.[11] Polyurethanes (PU) incorporated in the PDMS (e.g., Elast-Eon E2A, PurSil 35) have good durability and biostability, but are subject to hydrolytic degradation, which modulates the remaining strength.[12]

Polysiloxane elastomers are the most flexible materials and yet biocompatible, but the increased toughness, along with the increased recyclability, can only be realized by the application of sacrificial bonds or dynamic covalent chemistry at the cost of strength.[13] Block copolymer elastomers (SBS—Styrene Butadiene Styrene, SEBS—Styrene Ethylene Butylene Styrene, SIBS—Styrene Isobutylene Styrene, SIS—Styrene Isoprene Styrene) are rigid polystyrene domains and flexible chains which provide elasticity, adhesion, and mechanical strength, and which find application in electronics and in elastomer–metal systems.[14] Tribological extremes cannot be reached in all conditions. PU, made by using polytetramethylene ether glycol, is resistant to oil and hydrolysis, but, when the sliding velocity is high, when they are under tribological extremes and frictional heat, the molecular structure of PU will be changed, and this will influence its performance in the long-term.[15]

In this review, the nature of environmental degradation at elastomer–metal interfaces will be thoroughly explored with special attention to

corrosion, wear, and adhesion failures. The current study is based on a coupled chemo-mechanical–environmental model, unlike previous reviews, which tend to consider these modes of degradation individually; chemical aging, mechanical loading, and environmental exposure are regarded as dynamically coupled processes. Corrosion, wear, and loss of adhesion in the real-life service environment evolve in a synergistic manner, with interfacial chemical response shifting mechanical response and mechanical damage accelerating electrochemical reaction and transport. The purpose of this framework is to go beyond a list of degradation mechanisms and to instead synthesize the interaction between stressors and interfacial stability, life, and failure. Based on this, this review is a synthesis of the experimental observations, characterization methods, modeling methods, and mitigation measures to elucidate the causes of synergistic degradation and the rational design of durable, versatile, and sustainable elastomer–metal systems in industrial, biomedical, and electrical applications.

FUNDAMENTALS OF ELASTOMER–METAL INTERFACES

Interfacial Structure and Bonding Mechanisms

Elastomer–metal hybrid systems are becoming increasingly common in soft robotics, flexible electronics, and vibration-damping devices, where soft, large, elastic deformations must be combined with hardness and heat dissipation. However, elastomers are not tough and possess low thermal conductivity, which prevents their use in harsh environments subject to wear, corrosion, and adhesion, thereby hampering their durability. Enhancing conductivity and strength with typical filler reinforcements can compromise softness, making the optimization of multifunctional properties challenging. Recent studies have critically examined how interfacial coordination interactions help mitigate such trade-offs. Increasing toughness, stretchability, and conductivity ($2.35\ W\ m^{-1}\ K^{-1}$, $3496\ J\ m^{-2}$, $\approx 450\%$ elongation) are observed when silver-coated aluminum fillers and poly(lipoic acid)-based elastomers form AgS cross-links that create cross-linked networks.

Time-domain thermoreflectance demonstrated the mitigation of thermal resistance at the AgS interface, enhancing phonon transfer and energy dissipation under mechanical loading.[16] As an example of such dynamic coordination bonds, inspired by mussel adhesion, reversible stress redistribution is shown, which outperforms rigid covalent cross-links in measures of crack resistance and adhesion degradation under cyclic or corrosive loading.[17,18] In addition to nanocomposites, polymer–metal laminates combine the corrosive resistance and weight benefits of multi-purpose laminates, yet adhesion tends to be flawed in corrosive applications. Hot roll-bonding to fabricate Cr-coated steel–ethylene acrylic acid laminates has been shown to provide micromechanical interlocking, hydrogen bonding, and covalent bonding (–(O=)C–O–Cr, –C–$(O–Cr)_2$ between carboxyl (-COOH) and Cr_2O_3, by SEM, TEM, EDX, and ToF-SIMS. These powerful interactions strengthen bonding and are more resistant to corrosion and wear, thereby reducing the risk of delamination.[19] XPS also aids in explaining buried interface chemistry with spectroscopic techniques. Researchers have observed Al-O-C links in the Al/PMMA-b-P3HT interface, which reduced the mobility and nucleation bands on the surface.[20,21]

Adhesion Promoters and Coupling Agents

The permanent bonding of elastomers to metals has eluded coating, packaging, and structural composites because environmental conditions enhance failures through corrosion, delamination, and wear. Adhesion promoters and coupling agents provide stability to these interfaces by modifying chemical bonding, enhancing wetting, and increasing stress transfer. Promoters based on silane have also been investigated due to their capacity to covalently and hydrogen-bond-interconnect both elastomers and metallic oxidations. More advanced spectroscopy (including SFG-VS) demonstrated that 3-glycidoxypropyl trimethoxysilane and 3-GPS/MVS mixtures promote ordered methoxy orientation to enable silicone–metal adhesion, whereas non-promoting silanes (OTMS, TDFTMS) increase disordered structures, yielding no adhesion.[22] This molecular orientation is also essential in preventing moisture-assisted corrosion and delamination. The optimization of addition-cure liquid silicone rubber also accentuates the importance of functional silanes. Epoxy-, ester-, and urethane-silanes exhibited substrate dependence in their adhesion properties. EH-PHMS showed better results on aluminum and polycarbonate, while EP-PHMS demonstrated superior bond strength on glass, with a strength of over 1000%. N-PHMS, on the other hand, showed improved adhesion across all types of materials at ambient curing times. Improvements were connected to interfacial reactions, wetting, and molecular interactions.[23] In addition to functional silanes, primer systems are also widely used. 7-OTMS has been proven to bond silicone–aluminum, and cyanoacrylates improve the overall adhesion of elastomers. Nevertheless, primers have the disadvantages of solvent emissions and complicated processing. Silane promoters provide solvent-free versatility with improved adhesion to most polymers and metals (PE, PET, Cu, nylon, and epoxy), where they form stable molecular interactions with oxide surfaces, providing corrosion resistance (epoxy, ester, vinyl, phenyl, titanate, allyl, and boron silanes).[24–27]

In filler-reinforced elastomers, the coupling agents are also vital. In silica–polymer composites, silane treatment is observed to reduce the size of the silica network and alter particle dynamics, as evidenced by USAXS and XPCS, thereby decreasing hysteresis and increasing fatigue wear resistance.[28] The findings on vulcanized styrene–butadiene rubber (SBR) were corroborated by the study of similar anisotropic fillers, specifically silanes tuned to offer a reinforcement-damping trade-off in silane-reinforced rubber.[29] Silane-modified nanoparticles are also advantageous with polyurethane-based elastomers (PUEs). KH550-treated SiO_2, TiO_2, and Al_2O_3 nanoparticles enhanced dispensability, strength, and stability. The PUE arrives at Al_2O_3/PUE composites with tensile properties of 20.9 MPa, 1759% elongation, and thermal stability of 278°C.[30] These improvements reduce thermomechanical deterioration in damping and thermal protection.

Thermo-Mechanical Mismatch and Stress Accumulation

Elastomer–metal interfaces are prone to stress accumulation due to thermo-mechanical mismatch, which can enhance wear, impair adhesion, and propagate fatigue delamination, as shown in Fig. 1. The phenomenon has been of special concern in applications involving combined mechanical and thermal loading, such as seismic isolation systems, thermal interface materials (TIMs), and flexible or stretchable electronics. In structural isolation, as found in buildings and bridges, seismic loads are dissipated by utilizing elastomeric bearings. Depending on nominal elastomer properties, these devices are typical in design; however, important system parameters such as stiffness and damping vary with temperature. It is crucial to obtain an accurate measurement of the coupled thermo-mechanical behavior. Techniques to experimentally test this response, called real-time hybrid simulation (RTHS) methodologies, have been developed. In these arrangements, the elastomeric isolator is tested under direct conditions, and electromagnetic shakers are used to simulate the dynamic behavior of the superstructure. Environmental temperatures are precisely controlled using radiation heaters.

Experiments and simulations performed with RTHS demonstrated that temperature changes can have a profound effect on the dynamic response of the elastomeric system, and that thermo-mechanical mismatch contributes significantly to potential degradation pathways, including stress build-up at the interface and material fatigue.[31] Also, TIM performance under strain is highly dependent on compressive and tensile thermo-mechanical behavior. In stretchable and bendable devices, TIMs are often subject to large strain tension, although little has been done to determine how environmental conditions, including the level of strain, temperature, and cyclic fatigue, impact their structural integrity. Modifications in the thermo-mechanical behavior at operating temperatures may lead to local stress accumulations that can cause delamination, cracking, or thermal contact loss, which adversely affect long-term reliability.[32]

The effect of stress accumulation is also of paramount importance in the assembly of micro- and nanoparticles on flexible surfaces. Forced assembly methods, such as dry powder rubbing on elastic templates, enable the exploitation of the compliance of elastomers to alleviate stress concentration between particles in intimate contact. The compliance of the elastic substrates allows for wall deflection and bending around the particles, which minimizes local stress build-up and the development of defects during the assembly of large areas. The particle monolayers so assembled can

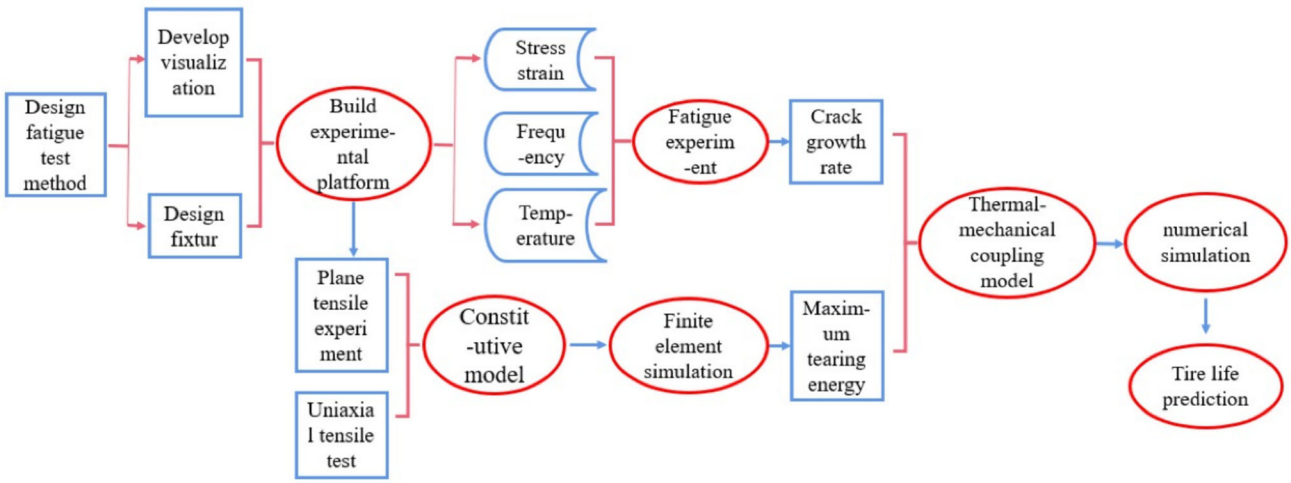

Fig. 1. Thermo-mechanical mismatch framework illustrating how coupled temperature and mechanical loading generate interfacial stress accumulation, fatigue damage, and crack growth, enabling lifetime prediction of elastomer–metal interfaces through experiment–simulation integration. Reproduced from Ref. 35 under the Creative Commons CC BY 4.0 license.

subsequently be transferred to flexible substrates, where they retain mechanical stability during deformation. This demonstrates that elastomer compliance can be designed to reduce stress-related failures at interfaces, which is crucial for maintaining adhesion and functional stability in photomasks, coatings, or hybrid electronic systems.[33,34] Unlike rigid templates, it is possible to cause excessive stress during the assembly of particles that are unequally sized or shaped due to overly rigid geometric constraints. Local wall deformation in elastomeric templates can absorb mechanical stress, resulting in defect-minimized monolayers formed even with industrial powder possessing large size and shape variations. These stress-relieving strategies are directly transferable to the elastomer–metal interface, as they demonstrate how compliance and elasticity at the interface can mitigate mechanical degradation and promote adhesion durability under cyclic or thermo-mechanical loading.[34]

ENVIRONMENTAL STRESSORS AND DEGRADATION PATHWAYS

Corrosive Medium in Salt Spray, Acids, and Industrial Pollutants

Exposure to corrosive environments is a leading contributor to the degradation of elastomer–metal interfaces, including loss of adhesion, wear, and mechanical failure. Investigations of weathering steel–elastomer joints revealed that a lot of the degradation in the hybrid is a result of exposure to the environment. Thirty samples of weathering (Cor-Ten), stainless steel (Inox), and carbon steel (S355) with varied rubber shapes were subjected to neutral salt spray, cyclic corrosion, and thermal aging. Force tests revealed that corrosion and age-related changes resulted in a decrease in both strength and deformation capacity, highlighting these aspects as important considerations for interfacial durability.[36] Polymers also degrade more rapidly in marine and saline environments, particularly in polymer–metal and composite systems. Salt spray decreased Mode I interlaminar fracture toughness (G_{IC}) in CFRP composites to 0.61 kJ/m^2 (SiO_2-CFRP) and 0.72 kJ/m^2 (PDA-SiO_2-CFRP) after 1 week, and to 0.5868 kJ/m^2 and 0.68 kJ/m^2 after 3 weeks in SiO_2-CFRP and PDA-SiO_2-CFRP, respectively. This was degradation by absorption of water, swelling, hydrolysis, and chain scission.

Hybrid reinforcements attenuated the damage: nanosilica and PDA-nanosilica retained 7% and 26% more G_{IC}, respectively, than did neat CFRP.[37] FPU coatings were sensitive to accelerated aging, as confirmed by UVA irradiation and salt spray. Spectral measurements demonstrated that samples exposed to 5 wt% NaCl under UVA exposure only experienced chemical and thermo-mechanical alterations, which could be detected by spectroscopic methods.[38] The effect of saline fog on dielectric properties and conductive properties has also been investigated. Under a conductivity fog condition (3 mS/cm), samples exposed at 0°, 10°, and 20° inclination angles experienced a change in electrical conduction pathways, which aggravated localized degradation due to the increase in moisture.[39] Other abuses to elastomers include chemical attacks that deteriorate the durability of the elastomers even further. Hydrogenated nitrile–butadiene rubber (HNBR) was reacted under aqueous H_2S and HCl, and chemical changes were determined using 13C NMR, XPS, and FTIR. New entities (C(=O) NH_2, C–S-C, C=S) appeared, and the H_2S exposure resulted in the most intensive mechanical destruction. The molecular degradation pathways were explained by radical-promoted C–S–C formation and a nucleophilic addition to C=S.[40] So, salt, acidic media, and industrial pollutants synergistically degrade elastomer–metal interfaces by corroding the metals, chemically aging the elastomers, and weakening interfacial adhesion. A mechanistic understanding of these stressors is vital for designing durable systems that can maintain long-term performance.

UV Radiation, Ozone, and Oxidative Weathering

Elastomer–metal connections in outdoor or high-performance systems, including but not limited to concentrator photovoltaic modules, are exposed to harsh conditions such as solar radiation, thermal cycles, oxygen, and moisture. These contributors compromise the adhesion, cohesion, and mechanical stability of the encapsulants, which influence the optical and thermal integrity over lifetimes exceeding 25 years.[41,42] Fracture mechanics-based methods are used to measure variations in adhesion/cohesion due to UV weathering. The short-term irradiation enhances adhesion energy due to the formation of new interfacial bonds, whereas long-term irradiation has the effect of embrittlement, resulting in loss of adhesion through photochemical cross-linking. High temperatures will enhance such effects. Coupled spectroscopic and mechanical characterization (XPS, FTIR, DMA) reveals that UV-assisted oxidative degradation is the dominant effect, allowing for predictive modeling of adhesion behavior as a function of UV dose and temperature.[43] Data obtained in the field support these findings: compared to UV-shielded modules, sun-exposed concentrated photovoltaic modules exhibit nearly half the adhesion energy. In contrast, dark thermal aging decreases adhesion energy through different pathways.[44]

Ozone and ultraviolet technology have added impacts on interfacial chemistry. Afterward, open visualization environment of PDMS generates a silica-like surface that improves wettability, electro-osmotic consistency, and binding in microfluidics; the optimal parameters depend on the diffusion

length and ozone concentration.[45,46] Just the same, thermoplastic olefins (TPOs) exposed to ozone, particularly to acrylic acid-grafted forms, acquire adhesion as a result of the introduction of polar functionalities. These enhancements are dictated by a combination of initiator type, exposure time, and surface chemistry, as revealed by attenuated total reflection (ATR), lap shear, and contact angle measurements.[47–49] PU films are microdomain structure-sensitive to both oxidative and enzymatic degradation in an oxidant environment, as well as to water permeability and oxygen diffusion. Ester linkages degrade more rapidly than urethane linkages, decreasing strain, tensile strength, and modulus.[50] At the nanoscale, magneto-rheological elastomers show time-dependent weathering. Atomic force microscopy (AFM) data taken over 9 months indicate that they initially gain adhesion/elasticity, then lose them, and continuously gain roughness.[51–53] Comprehensively, UV radiation, ozone, and oxidation processes interact with and contribute to the embrittlement of elastomers, as well as changes in interfacial chemistry and loosening of adhesion. Insights into both fast and natural weathering are crucial in the design of elastomer–metal systems intended for outdoor use and high-performance applications.

Temperature Cycling and Humidity Effects

In soft robotics, flexible electronics, and outdoor polymer systems, temperature fluctuations are crucial factors in determining the performance of elastomer-based metal interfaces and humidity. Elastomers such as EcoFlex 00-30, Dragon Skin 10, Smooth-Sil 950, and Sylgard 184 exhibit temperature- and humidity-dependent characteristics that can affect stressed capacitive sensors. Mechanical testing was carried out between − 40°C and 80°C and 5–95% relative humidity (RH), whereby high temperatures make it more rigid and decrease the strain at breakage. Humidity is less determinant in altering bulk mechanics, whereas electrical properties change, and need to be considered on a component-by-component basis.[54] TIMs applied to reduce interfacial resistance are also sensitive. Laser flash and sandwich-structure experiments indicate that most filled polymer TIMs maintain their conductivity during cycling, in contrast to gap pads and putties, which degrade around a transition temperature.[55] Combining mechanical/electro-mechanical characterization, Al-on-PI interfaces exhibit electromechanical fatigue, as in situ resistance tests reveal embrittlement due to grain growth, residual stresses, and poor adhesion.[56–58]

Structurally sound adhesively bonded joints are susceptible to thermal and humidity degradation due to residual stresses, curing shrinkage, and moisture absorption, and the consequent premature degradation in an adhesively bonded seat due to initiation of failure within the adhesive joint. Plasma treatments also improve adhesion through increased surface energy, but, again, the results vary depending on the substrate and the environment.[59] Silicone rubber used in outdoor/space applications deteriorates due to the combined effects of heat and humidity, resulting in oxidation, loss of hydrophobicity, and irradiation-induced cracking, which reduces insulation. Density and atomic oxygen resistance are optimized to enhance durability, and an accelerated aging process combining temperature, humidity, UV, and pollutants is related to natural aging.[60] Microscale measurements reveal that hygrothermal aging leads to the formation of pits, filler movement, and chain detachment, with the moisture content favoring hydrolysis and filler solvation.[61] Dielectric breakdown is also affected by environmental factors: increased moisture reduces the dielectric strength, and, in composites, the distribution and diffusion of stress, as well as the presence of elastomeric inclusions, compromise compressive integrity.[62,63] Dielectric elastomers exhibit shear modulus, damping, and permittivity that are influenced by humidity, with consequences for their long-term creep mechanism, vibration stability, and resonant frequency. Therefore, proportional ones should take into account humidity-dependent properties.[63] In general, elastomers subjected to thermal cycling and humidity have a higher stiffness, fewer failures at the point of failure, and system-specific electrical, thermal, and mechanical differences. Holistic characterization of coupled effects is necessary to facilitate the robust design of soft robots, electronics, and high-performance elastomer–metal systems.[64]

Synergistic Stressor Effects in Chemo-Mechanical Coupling

Elastomer–metal interface environmental stressors do not usually work singly. Corrosion, wear, loss of adhesion, and mechanical fatigue, in their turn, develop considering the chemo-mechanical coupling, when chemical reactions change interfacial bonding, transport, and mechanical properties, and deformation and wear of surfaces reveal new surfaces and increase the electrochemical activity. In the conceptual framework used in this review, interfacial degradation is considered to be a self-perpetuated mechanism: chemical aging and corrosion decrease adhesion and stiffness; mechanical deformation and wear enhance the formation and movement of defects; and thermo-mechanical mismatch increases further concentration of stress, facilitating crack initiation and propagation.

Elastomer–metal interfaces are also well-documented areas in which the interaction between chemical reactions and wear occurs. The combination of oxidative aging of elastomers with deformation accelerates fracture and wear, where oxidation of the material causes hydro-/chemo-mechanical interactions, leading to simultaneous interfacial

Table I. Chemo-mechanical coupling in elastomer–metal interfaces

Methods	Materials	Stressor coupling	Mechanisms	References
Covalent adaptable networks and constitutive modeling	Epoxy thermosets	Hydro-/chemo-mechanical interactions	Interfacial welding via entanglement and bond exchange; self-toughening and self-healing predicted accurately under multi-physical stressors	65
Constitutive plasticity model	Polymer electrolyte membranes	Mechanical cycling + chemical aging	Void evolution models lifetime; coupled degradation predicts durability of PEMs	66
Bio-based reinforcement	CNF- and chitin-reinforced natural rubber	Mechanical + interfacial chemistry	High-aspect-ratio CNFs enhance fracture toughness and covalent interactions without heavy surface treatment.	67
Phase-field modeling + modified Butler–Volmer kinetics	Lithium metal anodes	Electrochemical + chemo-mechanical stress	Ionic conductivity and SEI modulus govern uniform Li deposition; artificial SEIs designed for stable interfaces.	68, 69
Vitrimer welding and fracture modeling	Vitrimer interfaces	Chemo-mechanical diffusion + transesterification	Welding temperature, time, and cohesive region length control fracture and toughness evolution	70
Diffusion modeling in FE frameworks	Polymers under large deformations	Stress–diffusion–environment coupling	Both deformation-dependent and independent diffusion models capture multi-field coupling at large strains.	71
Viscoelastic/chemo-rheological analysis	Rubbers and liquid silicone rubbers	Vulcanization + chemical reactions	Viscous-to-elastic transition affects modulus and damping; foundation for chemo-thermo-mechanical load models	72
Tobolsky's extended two-network theory	Elastomers above $\sim$ 100°C	Thermo-chemo-mechanical aging	Chain scission + re-cross-linking drive creep, relaxation and permanent deformation	73
Functionalization strategies	Modified elastomers	Chemical tailoring + mechanical cross-linking	Tailored elasticity and toughness for high-performance silicone/rubber	74
Bergström–Boyce viscoelastic–chemo-mechanical framework	Liquid silicone rubbers	Large-strain viscoelastic + chemo-mechanical	Predictive accuracy up to 96% under temperature/stress; reliable lifetime prediction	75, 76
Multiphase continuum chemo-thermo-mechanical models	Polymer solids	Diffusion-driven aging + viscoelastic network reformation	Predicts long-term interface performance under service conditions	77

welding and topological entanglement, which cause increased toughness and self-healing through bond–exchange reactions, as summarized in Table I. An example of this is the responsive covalent networks found in epoxy-based systems, whereby hydro-chemo-mechanical interaction triggers concomitant interfacial welding and topological entanglement. Such multiphysical behavior has been modeled using constitutive models with the free-volume theory and rubber elasticity, which was verified by finite-element (FE) simulation and experiments.[65] Polymer electrolyte membranes can also be said to undergo coupled degradation, with cyclic stress and chemically driven aging (e.g., Fenton reactions) being explained by J2 plasticity models, with void growth being modeled as void growth under humidity cycling.[66] In this regard, bio-based nanofillers like cellulose nanofibers and chitin nanowhiskers provide viable solutions to reinforcement pathways that are sustainable, improving the fracture strength and adhesive power between surfaces without necessarily modifying surfaces.[67]

Chemical–mechanical coupling is also observed in electrochemically active systems. An example of the application of phase-field models to lithium metal anodes is the explicit treatment of stress-assisted ion transport and interphase evolution with modified Butler–Volker equations.[68,69] The modulus and conductivity of the solid electrolyte interphase determine the uniformity of deposition and the direct correlation between electrochemical stability and mechanical properties. Another such example is in Vitrimer welding, which is a diffusion-controlled transesterification reaction dominating the fracture

and healing behavior; microstructure-based models measure the effects of the cohesive-zone length on interfacial strength and welding kinetics.[70] Diffusion and the kinetics of the reaction are made even more difficult by large deformations, leading to the use of FE formulations that combine the deformation-dependent transport with boundary effects.[71]

Viscoelastic responses in both rubbers and liquid silicone elastomers are highly dependant on environmental exposure, cross-link density, and vulcanization conditions, and transitions in loss factor and modulus control long-term durability.[72] At temperatures that are higher than chemorheological (i.e., above 100°C), the prevailing and effectively modeled processes include stress relaxation, creep, and network scission reformation.[73] Elasticity, as well as durability, can be tuned using functionalization by incorporation of monomers, post-modification, or mechanical cross-linking.[74] Multiphase continuum models that combine degradation and network reformation have also been shown to exhibit predictive accuracies of 96%, similar to those of multiscale large-strain viscoelastic models (e.g., the Bergström–Boyce formulations),[75,76] whereas delayed chemo-/thermo-mechanical aging effects are also predicted by multiphase continuum models.[77]

Even though interfacial fracture energy (G- or J-integral) offers a strict measure of adhesion-dominated debonding in settings where degradation is caused by controlled loads, it is not universal between coupled degradation modes. Most of the environmentally-initiated failures, including corrosion-aided delamination, chemical, and abrasive or adhesive wear, do not creep through a single, clearly defined crack front. Rather, the degradation occurs by distributed damage, material removal, interfacial roughening, and progressive loss in cohesive strength, of which wear rates, friction coefficients, electrochemical impedance, or strength retention are more experimentally available. Fracture energy is time- and history-dependent in coupled chemo-mechanical conditions with reactions, diffusion, and viscoelastic dissipation permanently altering interfacial toughness. It can therefore be concluded that G-based metrics can be best applied when used with tribological, electrochemical, and aging descriptors and not as a universal parameter.

Combined, the discussed mechanisms in sections "Environmental Stressors and Degradation Pathways", "Corrosion Mechanisms", and "Tribological Degradation and Wear-Facilitated Corrosion" can be viewed in a single chemo-mechanical–electrochemical degradation map where environmental exposure triggers chemical and electrochemical reaction at the elastomer–metal interface, and mechanical loading and wear enhance the damage by creating local stress and heating the material through friction, respectively, and these two processes in combination, causing macroscopic failure in the form of delamination, material loss, and functional degradation. This unified system, which directly connects corrosion, wear, loss of adhesion, and mechanics via feedback relationships, is more rigorous than earlier reviews which considered each phenomenon separately, and offers a mechanistic foundation of lifetime prediction as well as the rational design of elastomer–metal interfaces able to survive multiple interacting stressors at the same time.

CORROSION MECHANISMS

Electrochemical Reactions in the Presence of Elastomers

Elastomeric matrices control the interfacial electrochemical reactions and so increase the mechanical strength and corrosion resistance of polymers and metals. Polymer electrolytes networks are elastomeric networks to improve their performance by using sodium complexation (lithium perchlorate) and branched ether terpolymers. Stoichiometry is able to increase the stiffness and temperature of glass transition and retain ionic conductivity through cross-linking via allyl glycidyl ether, which offers a 3- to 5-V electrochemical window.[78] In lithium metal anodes, chemically shielded interphases (ICE-SEI) on Li can be maintained at 40-mV overpotential over 10,000 cycles versus 400-mV bare Li in 750 h. The EIS shows reduced resistance, and pouch cells have 87% compared to 29% capacity retention, which depict elastomeric interfacial stabilization.[79] Electrochemical and dynamic-bond approaches can then result in tunable interfaces. Electric welding of polymer–metal composites is used to attain polymer–metal adhesion in a reversible way.[80] With the aid of triboelectric nanogenerators, electrolysis of seawater can be performed with cathodic protection, resulting in H_2, Cl_2, and NaOH, and the corrosion is also reduced (Tafel and EIS measurements).[81–83] The anti-corrosion behavior of dual-dynamic chemistries in the form of polymeric coating materials containing UPy and disulfide components is better. Added porosity and degradation of coating is associated with the decreased relaxation times (tau1, tau2) in the EIS-DRT analysis and can be used to provide mechanistic understanding.[84] Three-electrode EIS and neutral salt spray, which are classical methods, are still applicable to coating evaluation.[85,86]

The effects of real-time measurement of anionic contaminants are separated using membranes in ion-exchange and sensors, creating the interface capabilities of elastomers.[87] In wearables and flexibles, compliance and electrochemical stability are combined with conductive elastomers. The NBR-PANI composites provide reversible conductivity, toughness and processability to SSLMBs and

biotechnology electronics. Elastomeric electrolytes conductivity is higher than 10^{-4} S cm^{-1} and stability is 4–5 V or more, which means that they are safe to use with deformation.[88,89] Generally, elastomers can be successfully used in electrochemical, interface, and mechanical stability, leading to the creation of flexible electronics, energy storage, and bioelectronic corrosion-resistant, high-performance systems.[88]

This section does not contain lithium metal anodes or triboelectric nanogenerator (TENG) systems as application-specific digressions, but as model electrochemical interfaces explaining general principles that can be directly applied to elastomer–metal systems. Highly reactive metal surfaces in lithium metal anodes are stabilized by polymeric or elastomeric interphases, which mediate ion transport, inhibit local electrochemical reactions, and handle mechanical deformation; functions that are closely related to those of elastomers in both corrosion-resistant metal bonding and sealing. Likewise, TENG-based cathodic protection demonstrates the dynamic control of electrochemical reactions by mechanically active polymer–metal interfaces, providing design opportunities of self-powered corrosion inhibition and mechanically responsive protective coatings.

Collectively, the examples show that elastomeric materials can be used to offer mechanical compliance, electrochemical control, and interfacial stability simultaneously, which supports their applicability to the design of robust elastomer–metal interfaces in corrosive and mechanically aggressive conditions.

Electrolyte Percolation Through Elastomer Matrix

Elastomeric and polymeric coating barriers prevent corrosion due to their insulating and chemical protective capacities, but water movement through polymer films continues to be the main cause of delamination and interfacial deterioration.[90] Recent developments in self-healing, low-weight polymers, as well as graphene-based layers, demonstrate that understanding water diffusion is crucial for sustained protection.[91] High-temperature vulcanized silicone rubber, a typical material used in composite insulators, is prone to corona-induced degradation.[91,92] SR can be diffusion-controlled and is influenced by various factors, including humidity, temperature, filler content, tensile stress, thickness, and electric fields. High temperatures enhance its uptake, whereas hydrophobization and higher thickness impede it.[92,93] In nanocomposites, water transport occurs through the polymer matrix or filler conduits (hydrophilic). Hydrophobic systems (SBR/TW, PBD/TW) prefer diffusion through filler networks, and uptake and swelling will increase with an increase in filler loading.[94] Cellulose nanocrystals enhance permeability, making their percolating networks raise diffusion coefficients by an order of magnitude at high loadings.[95]

Kinetics are temperature and solution concentration-dependent. Higher solution concentrations decrease concentration differences, and hotter solutions increase ingress velocity. Filler leaching (ATH, fumed silica) changes the weight and permeability.[96] Langmuir-based models exhibit a dependence of permeation time on the sheath thickness, and adding moderate amounts of filler or treating the surface efficiently eliminates the transport. Nanofillers like graphene nanoplatelets and organo-clays stiffen the material but impede diffusion at percolation thresholds.[97–99] Examples of stretchable elastomer models include conductive aerogels in PDMS, such as PEDOT and PSS aerogels in PDMS (an elastomer stretches when in the non-conducting state).[100] The architecture phase, as in immiscible blends (ENR/PEO, ENR/PVdF), and ionic transport are determined by the phase architecture, which reduces percolation thresholds without sacrificing mechanical properties.[101,102] High-aspect-ratio whiskers (such as tunicate and ramie) strengthen matrices through hydrogen-bonded networks, which also regulate water transport.[103] Consequently, controlling electrolyte percolation and water diffusion through elastomeric matrices is fundamental to achieving corrosion resistance and prolonging life. The stabilization of polymer–metal dimensions with nanofillers, hydrophobic surface modifications, and designed percolation channels, along with regulated transport, provide routes to simultaneous strength and coordinated transport at the polymer–metal interfaces.

Galvanic Corrosion Triggered by Disbonding

Galvanic corrosion is one of the major degradation processes at metal–metal and metal–polymer interfaces, particularly under existing heterogeneities or disbonding. In Al/Cu systems, pitting on bond pads locally forms after the wafer saw, but untreated wafers are not affected; such is essential for Cu-containing Al alloys, such as PL455, in automotive applications due to their reliability.[104] Galvanic couples form at Al grain boundaries by Cu precipitation, thus creating pit nuclei. Exposure to deionized water at low temperatures, as well as nitrogen saturation, inhibits initiation, but halogen residuals left by CF_4 plasma enhance corrosion processes by promoting nucleation on Cu deposit crystals.[104] In fiber cross-over laminates, galvanic action between CFRP and steel in NaCl solutions causes production of ferric oxides and mass loss at the interphase. Debonding is the dominant mechanism of failure and can be modeled using a probabilistic fracture energy-based approach.[105] Fuel makeup also affects behavior: biodiesel is more conductive than gasoline or diesel, which accelerates steel pipeline corrosion. Using optical, SEM, and AFM, it has been found that soybean and sunflower biodiesel decrease the

weight and damage the surface of carbon steel and HDPE.[106,107]

Cross-sectional influence-averaged steel with 0.1-mm-based FML exhibits galvanic susceptibility in aerospace and automotive FMLs, such as GLARE and CARALL, due to electrochemical potential differences and CTE mismatch. The use of carbon fibers instead of glass fibers makes the parts stronger but corrosion-prone. Mitigation also decouples the components through the use of insulating layers (glass fibers, elastomers), relieving thermal strains, as well as increasing damping.[108,109] Elastomer filler in CARALL adds electrical resistant and flexibility that limits corrosion and maintains the bond. Mechanical testing and salt spray testing show a huge improvement compared to laminates without interlayers.[110] At the nanoscale, Cu/Ag nanoparticle-silicone extracts Cu ions via a redox mechanism, whereas Ag/Au systems are inactive due to the stability of gold.[111] In a biomedical interface, stainless-steel or NiTi orthodontic brackets undergoing the action of artificial saliva in stainless steel–NiTi or stainless steel–Shinye demonstrate preferential ion release. Stainless steel releases high levels of Ni and is localized in attack, posing a particular problem of galvanic effects in physiological media.[112] Galvanic corrosion of elastomer–metal interfaces is the result of electrochemical potential differences, electrical contact with an electrolyte, and interfacial inhomogeneity. Mitigation is based on the use of elastomeric laminates, insulating layers, and the selection of materials, as well as structural design to limit coupling layers and to provide robustness across the automotive, aerospace, energy, and biomedical sectors.

Time-Resolved In Situ Corrosion Studies

In situ characterization tools and real-time analysis are important for examining the phenomena of corrosion and interfacial reactions between an elastomer and a metal, offering information about molecular dynamics, corrosion, and degradation of polymer and nanoparticle kinetics. The primers play an important role in PU potting compounds that are used to shield the encapsulation. The interfacial signals of isocyanates have demonstrated that they disappear after 16 h of curing, therefore providing evidence of the formation of covalent bonds as the exclusive adhesion mechanism, which is in accordance with ATR-FTIR and peel tests.[113] SFG is a nonlinear optical process which provides structural specificity at submonolayers, enabling the optical interrogation of interfacial molecules by overlaying both visible and infrared lasers, which provides the chemical investigation of buried interfaces with subwavelength dimensions.[114] When NBR was subjected to 28 Mpa of hydrogen in a tribometer at high pressures, friction and wear were higher than in air or in argon, which has raised a concern about the compatibility of a hydrogen infrastructure.[115] The changes in nanostructures during corrosion, loading, or heating are monitored by small- and wide-angle X-ray scattering (SAXS/WAXS). SAXS allows the time resolution of nucleation to about milliseconds and, more recently, the strain on a polymer at the nanoscale would furnish real-time data on phase transitions that can influence interfacial performance.[116,117] Tension loading with Kevlar fibers entails fibril reorientation and lamellar domain transformation (SAXS) and by WAXS, and amorphous–crystalline transitions were detected at large straina to connect the nanostructure and macrostructure behavior.[118]

The SAXS and DLS of the geothermal waters have shown that the nucleation of nanoparticles ($\sim$ 3 nm) and their growth ($\sim$ 7 nm) occurs first-order kinetics irrespective of the ionic strength and temperature.[119] In situ absorption spectroscopy and GIXRD were used to explain the degradation pathway of $CH_3NH_3PbI_3$ perovskites under different humidity levels in thin films. The reaction with the proton transfer at the interface and the reduction of the reaction by hydrophobic coating mediated the ZnO/perovskite decomposition at the interface.[120,121] Time-resolved in situ methods, ATR-FTIR, SAXS/WAXS, and GIXRD, can be combined to clarify dynamic interfacial chemistry and nanostructural evolution, which will be beneficial in the rational design of advanced bearing-relevant coatings with enhanced adhesion, corrosion resistance, and long-term stability.

Perovskite thin films and lithium-based interfaces are mentioned as well-controlled model systems to investigate interfacial degradation under coupled chemical, mechanical, and environmental stressors on an interface in real time. Although the materials are not the traditional ones used in elastomer-based assemblies with metal, the degradation mechanisms, moisture-induced interfacial reaction, ion migration, phase decomposition, and stress-induced chemical transformation are directly comparable.

TRIBOLOGICAL DEGRADATION AND WEAR-FACILITATED CORROSION

Frictional Heating and Elastomer Breakdown

Frictional heating is a significant contributor to tribological losses in the contact between elastomers and metals. During sliding, increasing energy losses raise interfacial temperatures, which in turn influence friction and wear, especially on rough surfaces or when metals are textured and sliding velocities exceed 1 mm s^{-1}. Such solid models, including those with a viscoelastic dissipative mechanism and heating within nanometer-thin surfaces that can generate heat, demonstrate that heating results in an orientation-dependent tangential friction, which violates classical laws. Phase changes and tribochemical reactions can occur, for example, frictional melting produces lubricating films that reduce

friction on ice and snow. Massively influential analyses by Jaeger, Archard, and others developed models of moving heat sources, which were later applied to viscoelastic friction and finite substrate conductivity.[122–124] These predictions are supported by experiments, where a 2-mm-radius rubber ball sliding up on a smooth substrate resulted in temperature increases of ~ 10°C after 25 s and 20°C after 900 s, indicating flash temperature effects.[122,123] Seals manufactured from thermoplastic PU and nitrile butadiene rubber also demonstrate velocity-dependent characteristics. NBR exhibits lower surface temperatures and friction stability compared to TPU. The coefficient of friction is determined by the frictional-heating energy balance, modulus reduction, and shear strength, which are competing processes.[125–127]

Wear resistance is more than hardness. Reports on PU grades indicate that the tensile strength, elongation, and cyclic loading determine the erosion resistance. Residual strain and hysteretic behavior generated by plastic deformation and microstructural change under repetitive impact load are the same.[128] Thermal effects also influence dielectric failure. Silicone-based dielectrics in stretchable electronics exhibit temperature-responsive dielectric constants, conductivities, and breakdown strengths. Adding TiO_2 fillers enhances dissipation of heat and electrical stability by carrier trapping, but high temperatures may decrease homogeneity.[129] Generally, frictional heating couples mechanical, thermal, and chemical processes that determine wear and degradation of elastomers. These mechanisms are crucial in predicting tribological performance and maximizing the service life of elastomer–metal systems.

Abrasive and Adhesive Wear

Abrasive and adhesive wear are the primary dissolution mechanisms in elastomer–metal boundaries used in seals, tribological apparatus, and flexible systems, as described in Table II. The diversity of their development is linked to the nature of the lubricant, the material, and the topography of the surface. Block-on-ring tests demonstrate that under dry conditions, NBR, acrylic rubber, and fluoro-rubber exhibit different morphologies. The NBR has both scratches and ridges, whereas acrylic rubber and fluoro-rubber have almost exclusively scratches. Lubrication decreases ridge formation and debris agglomeration, most notably in acrylic rubber, but usually raises wear rates and also lowers peak friction coefficients.[130] Wear mechanisms that operate in elastomers include abrasive wear, fatigue wear, and roll-induced wear. Abrasive wear is caused by tearing on sharp asperities; fatigue wear is loaded on sharp asperities and deformation on smooth surfaces; and roll wear is loaded on smooth surfaces.

The coefficient of local friction determines dominance and is a reason that usually involves more than one mechanism.[131] This is demonstrated with PU elastomers; sliding contacts involving cast PU display a tensile-tear abrasive wear regime, whereas fretting is dominated by adhesive fatigue. Wear response is also varied due to stress, due to a combination of frictional heating.[132] Icephobic rubber and PU-based materials exhibit plasticizer-dependent durability; hard rubber is subject to greater wear loss, whereas 20–30% plasticizer as mass compromise provides both resistance to wear and ice adhesion.[132] Wear in composite elastomers exhibits a filler and particle dependency. Higher fiber loading contributed to increased wear in thermoplastic copolyesters reinforced with short fibers (carbon, PTFE, SiC, alumina) at high filler loadings, whereas lower wear was observed with large abrasives. Response surface methodology predictive modeling aids in the introduction to composite optimization.[133] PDMS wear in soft robotics is relative to the base–binder ratio and load. Moderate ratios (10:1) maximize resistance due to about equal microplowing/microcutting, whereas lower ratios reflect softer formulations that exhibit fatigue–abrasive wear under uniform stresses.[134] The particle size has been found to significantly influence NBR seals' transition from abrasive wear of the seals against SiC sandpapers to adhesive wear occurring with decreasing particle size, accompanied by a positive change in the friction coefficient.[135]

Niche applications include gecko-inspired adhesives and PDMS gel pads, which utilize both elastic modulus and solvent-mediated detachment to enable frictional control, albeit with minimal degradation at the nanoscale. In general, abrasive and adhesive wear are the combined (causative) influences of material, structure, and lubricant. Procedures focused on the specific selection of materials, reinforcement of composites, and surface engineering are needed to enhance the lifetime of the interface between the elastomer and metal.[136,137]

Synergistic Wear–Corrosion in Marine and Industrial

Tribocorrosion, or the combination of wear and corrosion, is an important issue that has severely constrained elastomer–metal contacts in marine and industrial machinery (bearings, gears, propellers, hydraulic assemblies, etc.),[138,139] as seen in Fig. 2. Austenitic stainless steels, such as 316SS, exhibit strength and resistance to chloride corrosion, but are susceptible to abrasive wear. BJP316 exhibited enhanced wear resistance due to the formation of a bronze phase as a solid bearing layer, as well as tribofilm formation by oxides, but at seawater corrosion rates up to 10 times higher than conventional 316SS.[140] Additionally, the

Table II. Abrasive and adhesive wear mechanisms in elastomer–metal interfaces

Methods	Materials	Wear mechanism	Key factors	References
Block-on-ring wear tests	NBR, acrylic rubber, fluoro- rubber	Abrasive wear with ridge/scratch morphologies	Dry NBR: scratches + ridges; acrylic/fluoro: mainly scratches; lubrication reduced ridge formation, dispersed debris, lowered peak friction, but increased overall wear	130
Mechanistic classification	General elastomer wear	Abrasive, fatigue, and roll-induced wear	The local friction coefficient dictates the dominant mechanism; mechanisms often coexist, complicating their isolation.	131
Sliding and fretting wear analysis	Polyurethane	Sliding to abrasive wear; Fretting to adhesive-fatigue	Scratch resistance is not directly predictive; frictional heating influenced wear behavior	132
Coating wear study	PU icephobic coatings	Two-body abrasion	Plasticizer levels (20–30%) optimized: softer PU lost more weight under abrasion; balanced wear resistance with reduced ice adhesion	133
Composite reinforcement and predictive modeling	Thermoplastic copolyester elastomers + fibers	Abrasive wear	Higher filler loadings increased wear; larger abrasive particles reduced wear; response surface models predict performance.	133
Wear in soft robotics elastomers.	PDMS (binder ratios)	Abrasive + fatigue wear	Moderate ratio (10:1) balanced microplowing vs. microcutting to higher wear resistance; softer PDMS to uniform wear, fatigue-abrasive mix	134
Particle-size controlled wear	NBR seals sliding against SiC sandpaper	Abrasive reversible adhesive transition	Smaller abrasive particle sizes led to adhesive wear; the friction coefficient varied with particle size.	135
Bio-inspired adhesion and solvent transfer	Microstructured adhesives, PDMS gel pads	Adhesive wear and controlled detachment	Elastic modulus and interfacial work of separation tuned frictional performance; solvent-assisted detachment preserved nanoscale structures.	136
Integrative strategies	General elastomer–metal systems	Abrasive + adhesive	Judicious elastomer selection, reinforcement, lubrication, and microstructuring mitigate wear while preserving interface durability.	137

CoCrFeMnNi and Al0.1CoCrFeNi high-entropy alloys exhibit better tribocorrosion properties in seawater sliding. The alloy containing aluminum has proven to have a stable passive layer and increased pitting resistance, which demonstrates electrochemical passivation as a promising way to mitigate corrosion.[141,142]

The kinetics of tribocorrosion are governed by environmental factors, including salinity, velocity, pH, and temperature. Potentiodynamic polarization with a factorial design substantiated that the synergy between corrosion and wear tends to dominate any other expected tendencies in material design.[143] Wear- and corrosion-compromising systems, such as FGMs and MMCs, have been engineered. Multi-layered Cr/WC/amorphous carbon coatings can be applied to offer stiffness, adhesion, and protection, leading to a positive wear–corrosion synergy.[144] The Mo_2NiB_2 hard-phase cermets enhance hardness and corrosion resistance, with the content in hard phases determining erosion–corrosion performance.[145] In H_2SO_4, carbon and stainless steels have been tested with corundum particles, and the material loss was found to be greater than the sum of erosion and corrosion losses, the synergy contributing between 32% and 99% of the damage.[146,147] Overall, tribocorrosion is an interdependent phenomenon involving both mechanical and electrochemical processes. Innovation of elastomer–metal interfaces, therefore, demands protection through coatings, composites, and interlayers that are capable of withstanding wear and corrosion in hostile environments.

ADHESION FAILURES: CAUSES AND CHARACTERIZATION

Environmental Aging and Interface Debonding

The fiber morphology of elastomer–metal bonding is a key factor in deciding the system-level durability of systems as large as a photovoltaic module or as small as co-molded polymer and metal assemblies. Interfacial structures are weakened in aging environments, cyclic loading, and exposure to high-temperature water, resulting in debonding and structural and functional performance corrosion. Recent studies by Fernandez and Spach have shown

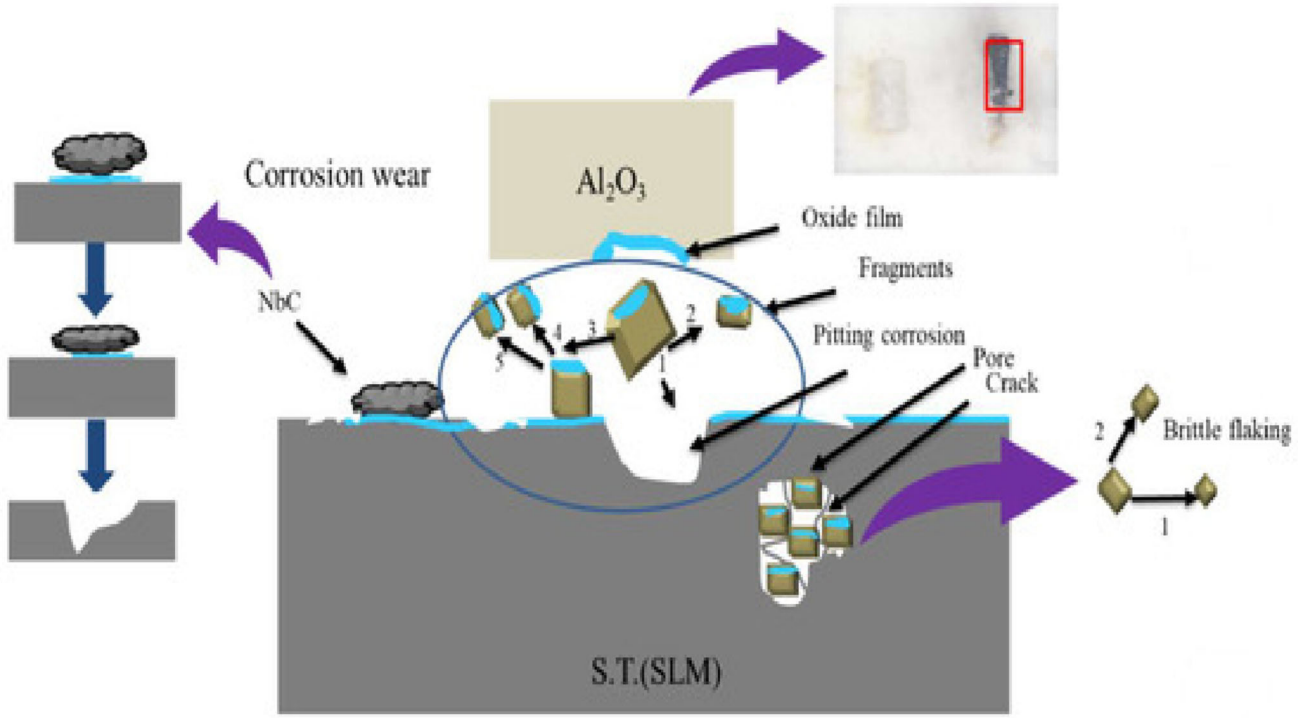

Fig. 2. Schematic of synergistic wear–corrosion mechanisms demonstrating how mechanical wear accelerates oxide film rupture, pitting, and brittle flaking, and explaining why corrosion rates and material loss exceed additive wear or corrosion effects in elastomer–metal systems. Reproduced from Ref. 148 under the Creative Commons CC BY 4.0 license.

that temperature cycling and moisture as well as applied stress considerably decrease the interfacial debond energy of PV backsheets. Debond energy reduced to 27 J m^{-2} in 750 h under solid-vapor aging conditions (85°C/85% RH), compared to an initial value of about 1000, and, under cyclic variations (±10°C, ± 20% RH), increased growth rates of debonds more than 500 times.[149]

Fracture kinetics models also associate debond propagation with the molecular relaxation process and are used to create accelerated aging experiments.[150] Water transport polymer relaxation, as well as interfacial chemical reactions, facilitates failures which are below the intrinsic fracture energy.[151,152] Test peels and overlap shear and rotary shear tests are commonly used to determine adhesion loss in damp-heat or UV conditions, but mixed-mode loading makes interpretation more difficult. Also, elastomeric systems such as silicone foams and TPU–metal structures fail at high temperatures and at temperatures below − 20°C because of creep, hardening, or loss of extensibility.[153] The infiltration of water and bond quality have a serious impact on the behavior of hydrothermal aging in fiber-reinforced elastomers and TPU–metal interfaces, and can be reduced by optimal deposition conditions and the application of silane coupling agents like γ-APS.[154] It has been reported that, in T700/HT280C/BMI polymer composites aged at 80°C/85% RH, debonding and delamination causes a reduction in stiffness and hysteretic energy loss through cyclic loading, resulting from debonding and delamination.[155] On a microscopic level, electrode–elastomer interfaces undergo staged fracture with crack nucleation, growth, and debonding controlled by the rate of energy release.[156] Similarly, elastomer–hydrogel hybrid functionalized surfaces are also vulnerable to oxygen permeability, surface aging, and infiltration effects which invalidate microstructured adhesion.[157]

Comparative evaluation of interface engineering strategies in reveals obvious trade-offs of durability, manufacturability, and environmental stability, where debond energies are reported to decrease by orders of magnitude during exposure to damp-heat conditions, as summarized in Table III. A more stable and industrializable solution with better retention of adhesion and protection against corrosion in cyclical environmental loading is provided by silane coupling agents that establish covalent bonds with metal oxides and chains of elastomers. Filler-based strategies, especially those using functionalized or dynamically interacting fillers, provide the largest benefit to long-term durability through improvements in interfacial toughness, fatigue resistance, and wear performance although at the

Table III. Comparative performance of elastomer–metal interface engineering strategies

Strategy	Durability	Manufacturability	Environmental stability	References
Surface treatments/primers	High initially; degrades under moisture and thermal aging	Moderate	Limited (humidity, UV sensitivity)	19, 113, 149, 154
Silane coupling agents	Good long-term adhesion retention	High (industrial scalability)	Good (moisture and corrosion resistance)	22–27, 154
Functional fillers	Excellent fatigue, wear, and toughness enhancement	Moderate (dispersion-sensitive)	High (thermal and chemical stability)	16–18, 28–30, 67
Self-healing/vitrimers	Damage-tolerant under cyclic and coupled stressors	Currently limited (processing/healing kinetics)	Excellent (adaptive bond exchange)	65, 70, 73, 77

price of a more complex formulation and processing. Self-healing and vitrimer-based interfaces are superior to damage tolerance to repeated and coupled chemo-mechanical damage via reversible bond-exchange reactions, but their broad use in industry is limited by processing temperature and healing rate.

Failure Modes: Cohesive Versus Adhesive Versus Mixed

Elastomer–metal interfaces bonded adhesively are appreciated for their high load-transfer efficiency, weight reduction, and ability to link dissimilar materials. Their failure can be classified as adhesive (at the interface), cohesive (within the adhesive), and mixed-mode.[158] Joint geometry, adhesive thickness, and mode of loading have significant effects on failure; e.g., mixed-mode cohesive zone models (CZM) of double scarf joints indicate that strength and energy vary with mode I and II parameters, as well as joint thickness and scarf angle.[159] CZM identifies adhesive behavior in terms of traction–separation laws that have parameters determined using load–displacement data.[160] Single leg bending tests yield mode-specific parameters in mixed-mode simulation. In asphalt and composite–metal joints, CZM in XFEM reflects the simultaneous occurrence of adhesive and cohesive cracks, with failure behavior controlled by loading rate, modulus, and fracture properties.[161]

Experimental studies validate the adhesive type, surface treatment, fillets and thickness as important factors. Standard fracture tests, such as the tapered double cantilever beam (mode I) and mixed mode bending (MMB, mode I/II), are used to determine strain energy release rates (G_I, G_II), and the applications of the Benzeggagh–Kenane criterion can be utilized.[162] Finite fracture mechanics theories predict the initiation of cracks in single-lap joints by using the tensile strength and fracture toughness, verifying the impact of adhesive thickness.[163] Film adhesives possess fracture toughness 30–60% higher than paste types; CZM also essentially reproduces mode I, but modifications are needed in mode II/mixed-mode.[164] These authors found that, on dissimilar substrates (e.g., steel/-glass), CZM laws in DCB/ENF, which are validated on lap shear, predict traction separation in modes I/II.[165] Prediction of the fatigue life is obtained in the form of triangular CZM laws that have been calibrated by DCB fatigue data.[166] Standard protocols (ASTM D5528-01 for DCB, ASTM D6671/D6671M-06 for MMB, and ENF tests) can be used to reliably characterize materials.[167] Inverse methods have been applied to adhesives bonded to aluminum, using CZM laws derived from materials such as Araldite AV138, Araldite 2015, and Sikaforce 7752.[168] The fracture toughness and interfacial bonding are enhanced in polymeric systems (PLA-TPU-PUEP blends), as verified by SEM and impact tests, due to the formation of PU-PLA copolymers.[169] In bioelectronics, interlocked hybrid electrodes (EMG/ECG recording) exhibit low interfacial impedance, a good signal-to-noise ratio, and robustness with TPU/Au electrodes.[170] Adhesive, cohesive, and mixed-mode failures depend on geometry, materials, and loading. Measurements and models, such as CZM, standardized tests, and interfacial engineering contributions, provide predictive methods for durably enhancing the elastomer–metal interface under stresses of both mechanical and environmental nature.

Interfacial Toughness Measurement Techniques

The mechanical integrity of elastomer–metal contacts is dictated by interfacial toughness and thus governs crack initiation, propagation, and adhesion life. Thermoplastics used (polypropylene; PP) are brittle at low temperatures; however, they can be made tougher with the addition of EPDM, EPR, PEO, SBS, or SEBS, but this modification results in a loss of tensile strength. Simultaneous improvement of tensile and flexural properties can be achieved through photo-cross-linking of PP/maleic anhydride-grafted SEBS (mSEBS) under UV irradiation, which provides a low-temperature interfacial strengthening route.[171] The incorporation of nanoparticles additionally improves the fracture

toughness. Amino-modified clays in an HNBR can enhance crack resistance over carbon black/graphite, highlighting the importance of filler geometry and interfacial chemistry.[172] Nanoclay/carbon black composites demonstrated that filler connectivity and entanglement were predictive of tensile strength,[173] as verified by TEM and electrical characterization. In engineering plastics, grafting functionalized elastomers with maleic anhydride or epoxy functional groups can be used to enhance adhesion/dispersion in PBT, thereby improving toughness.[174]

SBS blending with PA12/nanoclay enhanced adhesion and intercalate structures, and twin-screw extrusion enhanced adhesion and shear straining to generate toughening by cavitation and shear yielding.[175] Anhydride-modified PA6/CNF formulation was utilized in interfacial welding to enhance fracture toughness and electrical conductivity as well as thermal transport.[176] J-integral fracture mechanics assessed supramolecular self-healing elastomers and demonstrated a higher healing efficiency than tensile tests.[177] The addition of compatibilizers (MA-g-PP) reinforced olefin block copolymers with Kevlar fibers, oriented the fibers, and treated the surface, thereby increasing interfacial bonding and further enhancing tensile strength.[178] In PLLA/plasticizer blends, impact improvements were observed using zinc-catalyzed reactions at EBA-GMA phases, resulting in a dramatic enhancement of impact while maintaining crystallinity.[179] Selective concentration of nanoparticles at immiscible polymer interfaces, such as PLLA/EGD/MWCNT, resulted in enhanced adhesion and provided conductivity at low filler loading.[180] PDMS–hydrogel systems indicated that the cross-link density and secondary cross-linkers (TMSPMA) can control interfacial dissipation and peeling forces.[181] Hence, interfacial engineering through compatibilization, nanoparticle design and modification, and interfacial photo-cross-linking enables significant enhancements in failure toughness, strength, and adhesive durability in elastomer–metal systems.

AFM-Based Adhesion Mapping

Degradation under environmental and mechanical stresses, as well as nanoscale mechanical characterization of elastomer–metal interfaces, is a prerequisite for this study. Using AFM and nanoindentation probes, adhesion, stiffness, and viscoelasticity are measured with high resolution. PeakForce quantitative nanomechanical mapping quantitatively determines modulus and adhesion over interfacial zones. Dynamic vulcanization played a crucial role in enhancing the modulus and adhesion of thermoplastic elastomers and vulcanizates with fluoroelastomer phases (60–80 nm) in a polyamide matrix. In this system, interconnected rubber ligaments (4–12 nm) provided elasticity despite the presence of a plastic matrix.[182] Nanoindentation is used to measure the surface modulus (E) and surface hardness (H) based on contact mechanics. AFM-based mapping is used to measure the heterogeneity of nanofibers, composites, or PDMS films.[183–185] Higher orders of AFM, such as PF-QNM and FastForceMapping, can be used, which measure force–distance curves at each pixel, allowing nano-DMA experiments with frequency sweeps (10–2000 Hz) and bulk-compatible temperatures, offering a range of nano- to macro-mechanics.[186] Vice versa, in silica-reinforced rubbers (SBR, EPDM), HarmoniX AFM mapping provided evidence of filler effects, with local moduli of approximately 2 GPa, compared to 30–300 MPa in rubber matrices, showing nanoscale-bulk contrasts.[187]

The measurement of 3D modulus and roughness of a Sylgard 184 coating using the DMT modeling model complemented DMA values of storage/loss moduli, as well as tanδ.[188–190] AFM nanoindentation measured Young's modulus (3–4 GPa), hardness, adhesion energy, and interfacial fracture strength in porous crystalline materials like ZIF-8 nanocrystals using cube-corner indents at shallow depth.[191] So, AFM and nanoindentation provide qualitatively different information on adhesion, modulus, and energy dissipation of nanoscale elastomer–metal interfaces, which can be used to develop new, more form-permanent elastomer–metal interfaces and complement bulk measurements.

High-Resolution Synchrotron and Tomography

New synchrotron techniques enable the high-resolution probing of elastomer–metal interfaces, capturing structural, chemical, and mechanical properties across different length scales. Near-edge X-ray absorption fine structure, resonant scattering, and reflectivity can now provide moiety-specific contrast with $\sim$ 30-nm real-space imaging and sub-5-nm chemically sensitive scattering, which can be used to complement microscopy in examining interfacial organization.[192] X-ray computed tomography can provide non-destructive 3D imaging of delamination and impact damage in composites, which can be used to develop FE models for these materials. XCT imaging provides similar functionality to CT scans in metals.[193] Laboratory XCT is a fast-imaging method that can be subject to divergence artifacts.[194] Synchrotron-enhanced X-ray scanning tunneling microscopy can provide an atomic-scale view with chemical, electronic, and magnetic contrast through the precise alignment of the tip, sample, and beam.[195] Synchrotron-based scattering methods (SAXS/WAXS) enable the in situ observation of structure–property relationships under thermomechanical loadings, allowing for the connection of nanoscale strain deformations to polymer softening (temperature swings of – 10–0°C and

60–70°C).[196] Xene/rubber interfacial studies reveal that interfacial bonding can dynamically regulate self-healable strain-sensing behavior.[197] XRR, GIXRD, GIXF, and XPCS can additionally characterize flat interfaces and colloids.[198]

Synchrotron nano-CT has validated regular filling of MXene–elastomer fillers, mechanical stability (~ 4.93 MPa), and self-healing (~ 98%).[199] Neutron imaging and synchrotron X-ray computed tomography can help elucidate syringe fluid flow, including needle plugging.[200] Additionally, hard X-ray phase-contrast imaging can be used to image low-contrast structures, such as vertebral bodies.[201] Synchrotron radiation CT (SR-CT) provides a resolution of ~ 0.7 μm, which enables the characterization of fractures in short carbon fiber epoxy composites and the evaluation of treatment processes.[202] Combinations of synchrotron and tomography techniques deliver unparalleled insight into interfacial structure, damage evolution, and mechanics, providing a complementary relationship between nanoscale characterization and the macroscopic performance of durable elastomer–metal systems.

PREDICTIVE MODELING AND LIFE ESTIMATION

Finite-Element (FE) Models for Interface Stress Evolution

To study stress changes at elastomer–metal boundaries and to determine the behavior under complex loads and conditions, FE modeling is a requirement. It measures deformation, debonding, and degradation, providing insights into corrosion, wear, and adhesion failures, as shown in Table IV. Weak formulation-based FE has also been used to predict stress-driven dissolution,[203] and stress-driven interface migration can be used to model intragranular void evolution,[203] although aspects of including migration within interconnect lines suffer.[203] In soft elastomers, constitutive models are essential for actuators, haptics, and robotics, where viscous loss can occur due to both mechanical deformation and electrical polarization. The traditional FE considers only the mechanical actions, although coupled 3D electro-mechanical models have now become available to give accurate predictions in the case of alternating fields.[204] In the case of adhesive interfaces, cohesive failure, inelasticity,

Table IV. Finite element models for stress evolution and degradation at elastomer–metal interfaces

Modeling framework	Materials	Mechanism	Key outcomes	References
Weak formulation-based FE	Metal interfaces (dissolution studies)	Stress-driven dissolution	Predicted interface stress effects on dissolution; limitations in simulating inclusion migration	203
Stress-induced void evolution FE	Metallic interconnect lines	Intragranular void migration	Modeled stress-driven interface migration; challenges in inclusion evolution.	203
Coupled 3D electro-mechanical FE	Soft elastomers (actuators, robotics)	Deformation + polarization losses	Accurate prediction under alternating electric fields; surpasses purely mechanical FE.	204
Generalized cohesive FE with anisotropy	Adhesive interfaces	Cohesive failure, inelasticity, deformation jumps	Cohesive laws with coupled damage simulate adhesive layers under complex loads	205
Cohesive contact + Mooney–Rivlin hyperelasticity	Hyperelastic elastomers	Cyclic bonding–debonding	Predicted adhesion degradation, stiffness loss, and energy dissipation under cycling	206
Cohesive FE machining models	SiCp/Al composites	Matrix–reinforcement-tool interactions	Reproduced cutting forces, surface morphology in machining	207
Representative volume elements (RVE) FE	Multiphase polyureas (elastomer–glassy)	Strain-rate-dependent response	Captured glassy breakdown into microphases; predicted strain-rate effects on performance	208
Multiscale FE (maximum entropy + atomistic)	Irregular polymer–metal interfaces	Multiscale stress analysis	Enabled accurate analysis beyond the Cauchy–Born assumption; localized severe stress modeling.	209
FE for progressive cavity pumps	Elastomer-metal stator-cylinder	Adhesive failure and shear stress	Linked adhesion ratio, modulus, and pressure difference to interface failure; guided pump design	210
Plane strain FE + Newton–Raphson	Multilayer elastomeric bearings	Stress distribution and crack initiation	Predicted stress fields and crack initiation in laminated rubber-metal systems	211

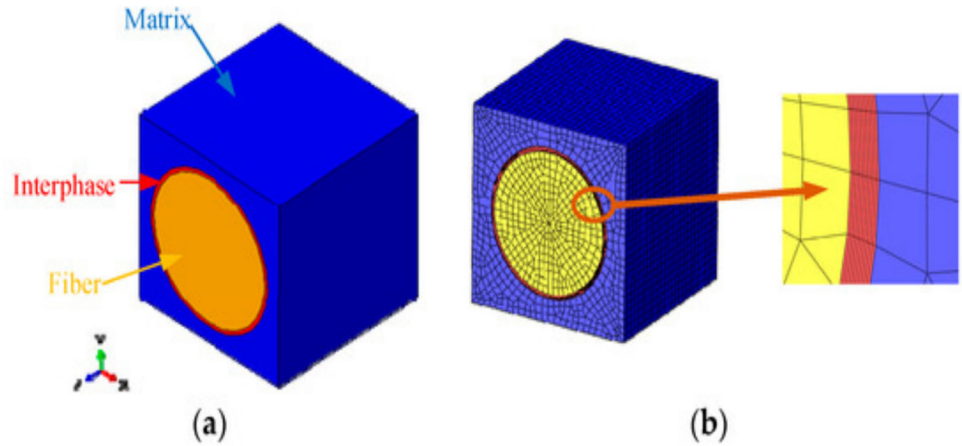

Fig. 3. Finite-element representation of a fiber–matrix system with an explicit interphase: (a) schematic geometry showing the matrix, fiber, and interphase regions; (b) discretized finite-element mesh highlighting the interphase zone and its local refinement used to resolve stress gradients and interfacial damage evolution. Reproduced from Ref. 212 under the Creative Commons CC BY 4.0 license.

and deformation jumps are described within a generalized FE framework, as shown in Fig. 3.

Damage variables that depend on each other, such as anisotropic cohesive laws, which are incorporated as Abaqus user elements, are applied to study an adhesive layer under complex loading and to reveal damage interactions.[205] A model of cyclic bonding–debonding in hyperelastic elastomers has been developed using recovery interface frameworks combined with bipotential contact and Mooney–Rivlin laws. These forecasts continued to deteriorate in terms of adhesion, energy dissipation, and stiffness decline, as well as broken cycles.[206] In composite materials like SiCp/Al, cohesive models can simulate the interactions between the matrix, reinforcement, and tool, as well as cutting forces, successfully modeling the tool morphology created during machining.[207] FE multiphase polymers take representative volume elements to model strain-rate effects in elastomeric–glassy segregated polyureas, and in the resultant plasticity-driven glassy fragmentation into new microphases and their effects on performance.[208] Multiscale FE is based on maximum entropy and discretizes moderate regions atomistically, treating severe zones with an FE method, thereby allowing the analysis of irregular interfaces that fall outside the framework of Cauchy–Born assumptions.[209] FE attributed adhesive rupture at stator–cylinder interfaces to shear strain, adhesion ratio, modulus, and pressure difference in pumps, helping to optimize the design of progressive cavity pumps.[210] In multilayer systems, the stress distributions can be predicted using FE (e.g., with plane strain elements and Newton–Raphson solutions), leading to the initiation of cracks in laminated rubber–metal structures.[211] All these studies highlight the predictive capabilities of FE modeling in predicting interfacial stress, multiphase system response, as well as the design of robust elastomer–metal components that are less susceptible to corrosion, wear, and adhesion degradation.

Digital Twins for Elastomer-Metal Interface Systems

Digital twins (DTs), virtual replicas of physical systems, can be a formidable tool in simulation, monitoring, and predictive evaluation of elastomer–metal interfaces. DTs have seen wide application in the aerospace industry by NASA and the USAF with the aim of using them as model-based multiphysics simulations to encourage proactive maintenance and to mitigate failure.[213] In production, DTs come together with IoT, cloud, big data, and artificial intelligence to facilitate smart processes. Unlike the cyberphysical systems, DTs can effectively translate physical processes into a high-accuracy representation and forecast the degradation of interfaces and detachment rates in the presence of operational environments.[214] In combination with machine learning, DTs enhance the optimization, accuracy, and sustainability of additive manufacturing and materials processing.[215] In addition to production, DTs aid in civil infrastructure and sustainable energy. As another example, TENGs coupled with DT-enabled structures can achieve self-powered sensing over time, continuously monitoring the wear of elastomeric elements.[216] In bioengineering-related matrices, DTs predict delamination and corrosion of implantable devices, including cochlear implants, where coupled diffusion interface models are used to model in COMSOL with high experimental agreement.[217]

The ML-enhanced DTs support physics-informed computational optimization of energy and hydrogen infrastructures, predicting the failure in metallic, ceramic, and elastomeric interfaces.[218,219] At the lower levels of the homogenization–localization multiscale DT frameworks (calibrated against experimental data), hierarchical predictions of

mechanical behavior, wear, and sticky film degradation can be made.[220] The DTs can be further extended to structural health monitoring, healthcare, and smart environments through AI-enabled sensors connected to edge and cloud computing, allowing for the predictive detection of corrosion or debonding.[221] One way in which DTs can address the evolving state of the interface is through hybrid DTs with parameter sharing and transfer learning, which have been applied to resilient infrastructure monitoring, as exemplified by localized degradation setting and adhesion failure prediction.[222] On the whole, DTs offer real-time tracking, simulation, and dynamic control of the e–m operational interfaces, thereby achieving durability in industrial, biomedical, and structural systems.

MITIGATION STRATEGIES AND SURFACE ENGINEERING

Surface Pretreatments and Primer Technologies

Strong elastomer–to-metal adhesion is conditional upon good surface preparation and the use of primers. There are two outcomes resulting from the interfacial bonding between the primer and the surface chemical bonding and mechanical stabilization. The composition plays a significant role in determining the performance. The VTMS/TPOS/TTB primer formed a robust metal bond but compromised cohesion due to adhesion to silicone (AA6061), whereas an SiH oligosiloxane/vinyl–PDMS/platinum/silica system exhibited greater cohesive strength at the primer/elastomer interface, with weaker metal attachment. The most effective formulation combination of silanes, vinyl silicone gum, hydroxy-PDMS, and silica fillers, when used together, yields the highest strength with cohesive elastomer failure. Silica fillers reinforce the silane/vinyl silicone gum matrix and also enhance adhesion.[223] The roughness of the substrate and the chemistry of the primer governs adhesion. AA6061 can be hydrolyzed and condensed by silane-based systems to achieve very high levels of cross-link density, resulting in cohesive failure, except that an overly rough surface interferes with adhesion. This is achieved through a two-component approach, utilizing active silanes and reactive silicone chains, which deliver predictable adhesion over a range of surfaces.[224]

Cyanoacrylate-based precursors produced nanostructured coatings, which were thin and porous on silicone rubber, with porosity and secondary bonding dependent on the solvent used.[26] Flexibility during forming operations was provided by automotive primers that utilized high-molecular-weight, low-cross-link-density elastomeric polyester resins.[225] In magnetorheological elastomers, silane-modified iron particles were able to enhance the particle–matrix bond, thereby increasing stiffness and inhibiting debonding.[226] Cycloaliphatic diepoxide primers were superior to silane primers in metal wire bonding to TPU, and were faster to process, while also showing improved hydrothermal stability.[227] Surface pretreatments also eliminate contaminants and oxides, as well as modify surface chemistry, as shown in Fig. 4. Abrasion and blasting are inexpensive, but can cause damage. Lasers provide selective cleaning, but are still expensive. Plasma exposes the surface to oxygen groups, which enhance surface energy, wettability, and adhesion.[228] In polymers such as polypropylene, abrasion enhances surface polarization and energy; however, pretreatment of the samples with air plasma can further increase surface energy and the fracture of polar bonds, resulting in enhanced adhesion.[229–231] Combining plasma- or mechanically-treated aluminum with sol–gel coats, primers, and regulated adhesive curing (as in the FM 300 K films) yields reproducible adhesions under known thermal and pressure conditions.[232] Industrial coatings are used that include multi-coatings (two-coat epoxy primers and weather-resistant topcoats), as well as PU topcoats for corrosion resistance. Solvent-based systems are also being replaced by waterborne PU in an effort to reduce VOCs and comply with environmental regulations.[233]

Nanostructured Barrier Coatings and Functional Interfaces

The innovation of nanostructured barrier coatings and functional interfaces is critical to improving the durability and environmental resistance of elastomer–metal systems. Nanostructured networks in elastomer composites enhance the electrical, mechanical, and adhesion characteristics, while also acting as a barrier against corrosive media. In natural rubber with segregated graphene networks, fabricated by ice-templating, very low electrical percolation thresholds (0.4 vol%) were achieved, compared to those of homogeneous NR/graphene (3.6 vol%). These composites demonstrated outstanding sensing ($\sim$ 6700 liquid responsivity, $\sim$ 114 s response), reproducibility and stability under 60% strain in 400 active–active bending cycles.[235] Segregated networks also eliminate stress at interfaces, which can lead to mechanical and environmental denaturation. Superhydrophobic and hydrophobic nanostructured coatings prevent the occurrence of corrosion and protect metals from exposure to moisture.

Nano-sized particles of alumina or silica enhance scratching resistance, titania and ZnO provide UV-blocking and anti-microbial effects. Nano-ZnO-modified PDMS showed low sliding angles and water contact angles around 168° and effectively repelled water and oils at the junction of elastomers and metals.[236] Nanostructured polymer composites provide enhanced gas and dielectric barriers, which are crucial in automotive and packaging applications. The long-term stability is ensured through fillers

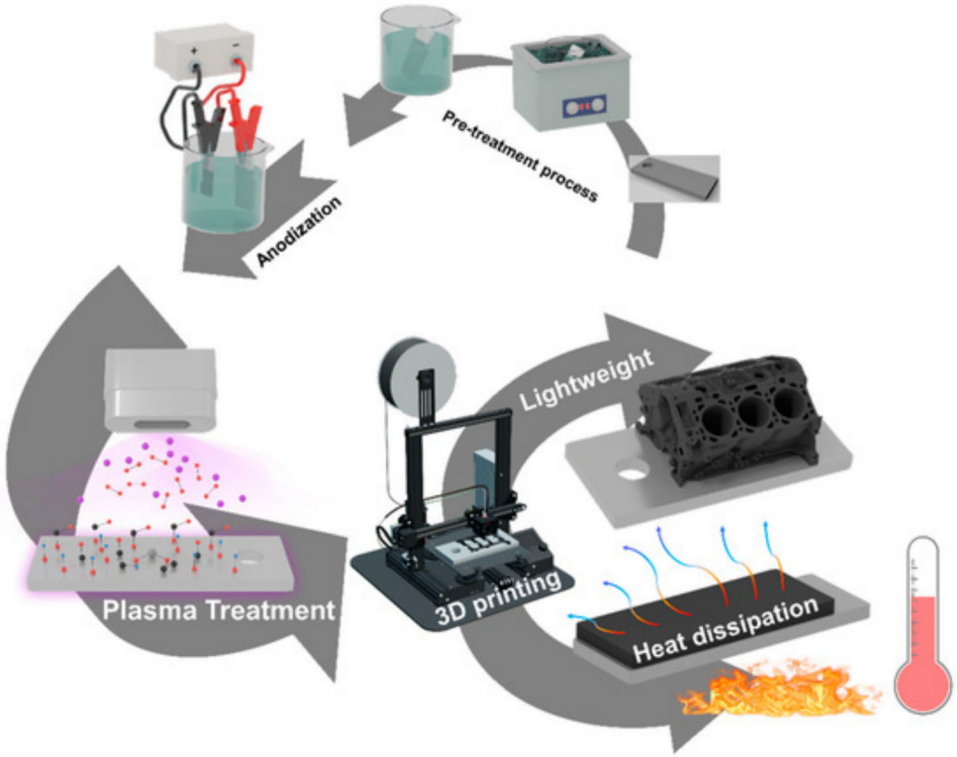

Fig. 4. Surface pretreatment and plasma-assisted modification strategies for elastomer–metal adhesion. Reproduced from Ref. 234 under the Creative Commons CC BY 4.0 license.

like POSS and clays uniformly dispersed therein. For example, VA–polyamide nanoblends exhibited substantially improved barrier and dielectric resistance.[237] The fabrication procedures reinforce interfaces. Micro-/nano-textured molds used in injection molding yielded superhydrophobic finishes (contact angles $> 150°$), and were less prone to wetting and corrosion.[238] Hierarchical lotus-like textured materials were created by laser-ablated geometries that adhered and were anti-delaminating under strain.[239] In conductive elastomer composites, 3D carbon nanostructure networks afforded enhanced conductivity compared to composites with the same loading, but offered high elongation that facilitated piezoresistive sensing to detect early onset interphase degradation.[240] Conductivity and impedance were strongly dependent on dispersion and orientation of the GN nanoplatelets.[241,242]

Conformal thin-film nanocoatings released with ALD inhibit moisture and/or electrolyte reactions, are stress-resistant and can accommodate volumetric changes. These types of ALD barriers directly translate to the mitigation of corrosion, wear, and interfacial degradation in a manner similar to that found in elastomer–metal cases.[243] In total, nanostructured coatings and functionalized interfaces contribute to enhanced levels of fracture resistance to corrosion, wear, and mechanical strain, thereby prolonging the service life of elastomer–metal systems.

Elastomer Formulation for Enhanced Compatibility and Durability

Formulation governing corrosion resistance, wear, and stability of adhesion at elastomer–metal interfaces are decisively decided by elastomer formulation by coupled mechanical and environment stressors. Natural rubber has been used due to good elasticity and damping, although constraints in supply and environmental resistance have prompted the introduction of synthetic and bio-based elastomers based on the butadiene, styrene, isoprene, chloroprene, and ethylenepropylene chemistries, and in which interfacial life is regulated by polymer chemistry, network structure, and filler–matrix interactions.[244] Compatibilization techniques, e.g., LA/TPU blends, PU-PLA copolymers and SR/EPDM formulations enhance phase morphology and interfacial bonding, minimizing delamination and degradation in aging during cyclic loading.[169,245] Likewise, silicone elastomers can be cured under control to allow network integrity to be balanced with the long-term performance of adhesion.[246]

Filling systems and novel processing directions also increase the resistance to coupled wear and chemical degradation. Graphene-reinforcing and carbon nanotube (CNT)-based materials could enhance the thermo-oxidative stability, cohesion, and stress transfer when uniformly spread using a solvent-casting method or freeze-drying

method.[247–250] Stress relaxation and damage tolerance can be achieved through dynamic network designs, such as vitrimer-like systems with epoxy-functionalized fillers, which allow crack formation to be alleviated during repeated loading and environmental exposure in the environment.[251] The examples of shape-memory and biodegradable elastomers also show that network design can be used at the same time to promote the durability of adhesion, mechanical recovery, and biocompatibility in the challenging service environments.[252–254] An example of the success of the formulation-based durability improvement is highlighted in the case of phyllosilicate-filled butyl rubber compounds that have higher barrier capacity, hydrophobicity, and chemical degradation resistance. SEM analysis prior and subsequent to the abrasion testing process as illustrated in Fig. 5 shows that phyllosilicate-filled vulcanizates have a more coherent surface morphology than unfilled systems, implying that they are more resistant to decomposition by abrasion damage.[255] The resulting polymer–filler interactions that lead to the increase in the hardness and density of cross-linking, without excluding,

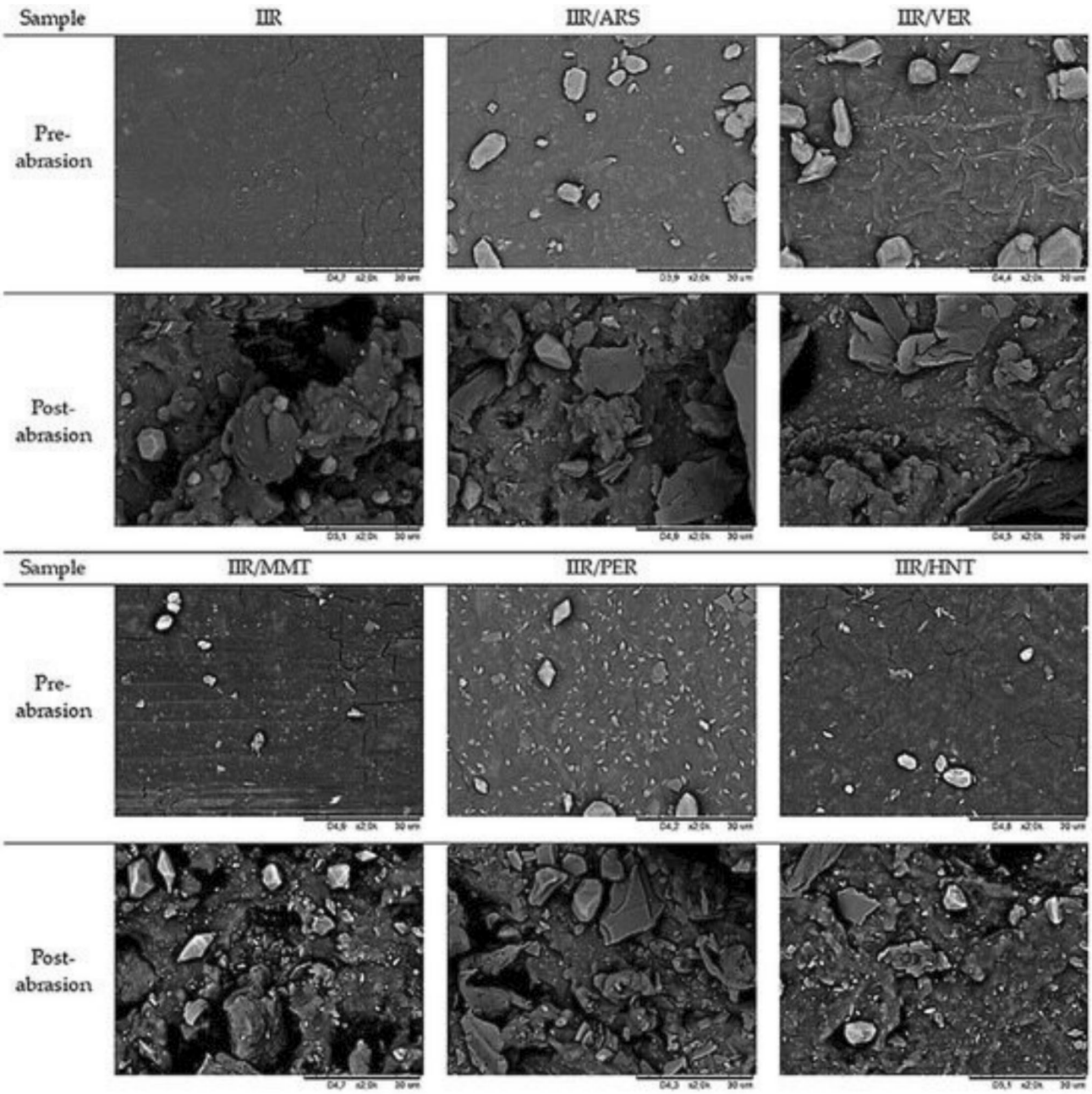

Fig. 5. SEM images of phyllosilicate-filled butyl rubber before and after abrasion, showing filler-dependent surface damage and improved abrasion resistance due to polymer–filler interactions. Reproduced from Ref. 255 under the Creative Commons CC BY 4.0 license.

improves the performance of the barrier but can also result in an increase of mass loss due to abrasion with increased filler loadings, thereby emphasizing the trade-off between stiffness and wear resistance. The findings highlight the significance of elastomer formulation optimization, i.e., balancing the content, dispersion and network formation of the filler to provide durable elastomer–metal interfaces, which can prevent corrosion, wear, and adhesion degradation all at the same time.

Green and Sustainable Anti-corrosive Systems

Green and sustainable anti-corrosive measures are becoming relevant towards improving the life of elastomer–metal interface subjected to coupled corrosion and wear and adhesion stressors. Traditional Cr- and Zn-based finishes or biocide finishes are more based on traditional barrier protection and high initial adhesion, yet they have environmental issues and tend to become irreversible upon microcracking, plastic deformation, or chemical corrosion. Conversely, novel sustainable systems that are grounded in carbon nanomaterials, bio-based polymers, and adaptive chemistries provide multifunctional protection, as they enhance all aspects of corrosion protection, mechanical strength, and interfacial stability under service-relevant conditions.

Graphene oxide and carbon nanotubes are the examples of carbon nanomaterials that were added to PU, epoxy, and elastomeric matrices to confer chemical inertness, mechanical reinforcement, UV resistance, and antibacterial properties. Hierarchical networks made of conductive TPU/CNT/PDMS composites, can protect elastomer–metal interfaces against moisture and acidic and alkaline conditions through cyclic loading without compromising modulus, elongation, and electrical conductivity.[256] Nitrogen-doped CNT derivatives and graphene further increase the coating stability and corrosion mitigation by improving interfacial bonding and continuity of barriers.[257] Such versatile nanocomposites are thus better than traditional stiffer coatings in combination mechanical and chemical stressor conditions. Bio-based polymer systems have built-in hydrophobicity, corrosion inhibition, and adaptive-damage tolerance. PDMS-modified acetylated starch-based PUs enhance transparency, liquid resistance, and anti-smudge effects, coupled with reducing corrosion reactions.[258] Sustainable cashew nut shell liquid-derived PUs and other plant-oil-based systems have high contact angles (112–121°), biodegradability, and microwave-activated self-healing (some cases) which allows recovery of protective functions following mechanical damage and orders of magnitude reduction in the rate of corrosion in steel.[259] Further enhancement of interfacial film stability and wear resistance with hydrogen bonding and boundary lubrication mechanisms is achieved with sustainable tribological approaches, such as the use of lignin-containing ionic liquids as lubricants and vegetable-oil-based machining fluids.[260,261] Thiol-, wax-, oxide-, and polysiloxane-based fluorine-free superhydrophobic coatings also offer anti-biofouling, self-cleaning and anti-icing functionality and do not have environmental persistence issues.[262–264]

Bio-based and self-healing systems are found to be more resilient to long-term coupled stressors such as corrosion, wear, mechanical cycling, and exposure to the environment compared to conventional ones. Whereas conventional coating schemes degrade gradually as defects are created, dynamic bonding schemes, reversible covalent networks, or self-healing mechanisms are able to partially re-establish mechanical integrity and interfacial bonding during service. It has been experimentally demonstrated that bio-derived PUs, lignin-, starch-, and carbon nanomaterial-reinforced elastomers maintain mechanical properties, conductivity, and corrosion resistance under cyclic loading, humidity, and chemical exposure, and, at the same time, they lower wear and frictional damage.[256–260] These systems have definite advantages over their non-dynamic barrier-based counterparts, despite the fact that there are still challenges associated with healing kinetics, scalability, and complexity in processing.

The efficacy of sustainable coatings in corrosive environments is also supported by the electrochemical evidence. As shown in Fig. 6, when using ELO-LnK composite coatings, they show a distinct shift of the open-circuit potential (OCP) towards most positive values in a 3.5-wt% NaCl solution, i.e., it also has an enhanced corrosion resistance compared to unmodified coatings.[265] LnK-based coatings

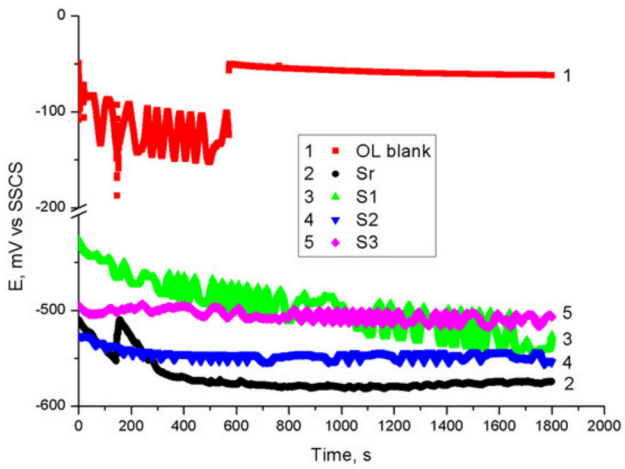

Fig. 6. Open circuit potential (OCP) evolution of ELO-LnK composite coatings on carbon steel in 3.5-wt% NaCl, showing a positive potential shift and faster stabilization with increasing LnK content, indicative of reduced porosity and enhanced corrosion resistance compared to the unmodified coating. The results demonstrate the effectiveness of bio-based modifiers in stabilizing elastomer–metal interfaces under corrosive conditions. Reproduced from Ref. 265 under the Creative Commons CC BY 4.0 license.

containing higher LnK contents exhibit more stable potentials and faster reaching of the potentials, i.e., less porous and better barrier properties in the presence of prolonged exposure to the electrolytes. Cumulatively, carbon nanomaterials, bio-based polymers, and ionic liquid-based systems are all environmentally friendly, mechanically stable, and electrochemically active materials to reduce corrosion, wear, and adhesion degradation of elastomer–metal interfaces under realistic and multi-stressor service environments.[256–265]

APPLICATION-SPECIFIC CASE STUDIES

Automotive Mounts and Seals

Automotive mounts, seals, and gaskets featuring elastomer–metal interfaces are subjected to harsh conditions, where environmental stress affects their long-term reliability, as illustrated in Fig. 7. Such parts achieve vibration isolation, acoustic damping, and protection against contaminants, but are easily affected by fatigue, temperature variations, and corrosion. Vehicle door seals have a direct impact on acoustic comfort, as sound transmission loss is influenced by the viscoelasticity of the elastomers and their structural adhesive behavior; a study found that hyperelastic and viscoelastic material properties relate to sound transmission loss and that a scale of degradation suggests a reduction in sealing efficiency.[266] Liner hanger assemblies in oilfields are supported as examples of industrial seals that fail. EPDM and NBR show good resistance to pressure testing, but CO_2 exposure causes severe degradation and leakage.[267] HNBR in hydraulic fluids, when subjected to high temperatures and compression, exhibits cross-linking, oxidative embrittlement, and adhesion loss.[268] Failure tests based on pressure–extrusion curves and transparent chamber tests can be used to correlate pressure drop and extrusion with the initiation of cracks and energy release rates in fractures, allowing the prediction of adhesion loss under cycling.[269] The potential weakness of conventional elastomers are compounded by their intrinsic weakness. Degradation exposure to high temperatures or excessive rigidity results in loss of strength, leading to wear, brittleness, and delamination.

Bone-like materials and conductive, biodegradable elastomers can expand biomedical applications to electronics, although bonding is sensitive to oxidizing, thermal, and hydrolytic environments.[270,271] The thermal transitions also regulate durability: by hardening (above room temperature), the chain flexibility permits recovery to take place; however, when below room temperature, stiffening and microcracking result, leading to bond degradation. To monitor such effects, DMA and compression set studies are conducted.[272,273] To combat these losses, thermoplastic vulcanizates possess melt-processability with elastic restoring behavior, oil resistance, and stability at thermal extremes, providing greater adhesion durability in car seals and isolators.[274,275] Despite optimistic statements about tribological degradation, in the case of seals contacting metals or glass, vibrations are likely to accelerate wear, noise, and microcracking, a reason to focus on advanced material and surface engineering.[276] Overall, elastomer–metal interfaces fail due to coupled mechanical, thermal, and environmental processes. Corrosion, oxidative aging, wear, and

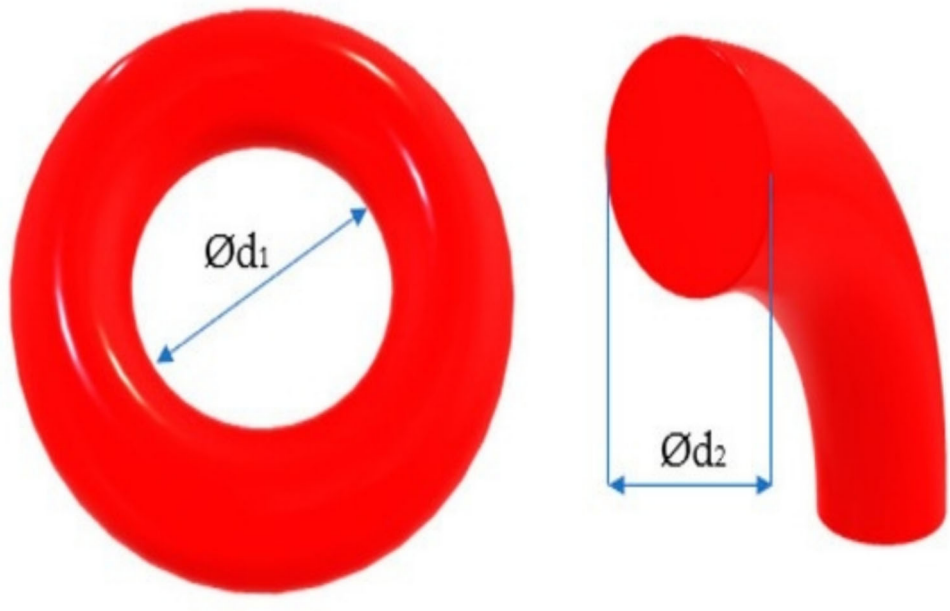

Fig. 7. Geometrical models of automotive elastomer–metal mounts and seals. Reproduced from Ref. 277 under the Creative Commons CC BY 4.0 license.

adhesion loss are closely related to operational stresses. Geometrical optimization, modeling, and diagnostics, as well as new formulations, are still enhancing the seal durability in harsh conditions.

Aerospace Vibration Isolation Systems

In aerospace systems, vibration isolation is crucial to ensure a particular system remains stable under extreme conditions. Metal-bonded elastomer isolators are commonly deployed due to their efficiency and flexibility, but are constrained by the effects of environmental factors on the thermo-mechanical robustness of the elastomer isolator, which can lead to degradation, oxidative degradation, vacuum-induced degradation, and radiation embrittlement. Pioneering efforts by Vaillon and Philippe with spacecraft flywheel isolators achieved $>$ 40 dB at resonance and $>$ 50 Hz; however, long-term space effects, including loss of adhesion and radiation-induced degradation, were concerning.[278] Researchers reported cantilevered flywheel suspension systems that rejected vibrations above 100 Hz but could not withstand the low-frequency degradation associated with elastomer bond stiffening under vacuum and high temperatures.[278] Smart elastomers, particularly magneto-rheological elastomers (MRE), enable tunable stiffness and damping through the application of magnetic fields. MRE pads incorporating several ball transfer units offered adjustable restoring forces in both simulation and experiments.[279] Oxidation, fatigue, and humidity-induced swelling of the particles, however, deteriorate particle–matrix interfaces, decreasing controllability. A similar problem has been observed in automotive MRE suspensions under two such loads, thermal and cyclic.[280] MRE isolators, referred to as quasi-zero stiffness (QZS), improve low-frequency attenuation through the use of MRE-negative stiffness units.[281] However, cyclic shear results in interface wear and delamination, as seen in QZS incubator systems, where nonlinear stiffness changes were attributed to elastomer aging.[282]

Complex MRE structures, such as multilayer, bi-directional shear,[283] and shear-compression hybrid geometries,[284] can provide tunable damping but remain vulnerable to the premature onset of micro-cracking, adhesion loss, and crack propagation through bonded interiors. Vibration-driven motion with regolith transport has been demonstrated in alternative dielectric elastomer actuators (DEAs);[285] however, these actuators experience electrochemical decomposition and interfacial failure upon exposure to radiation and repeated heating and cooling. The choice of isolator material also offers possibilities for damping mechanisms, including viscoelasticity and crack energy dissipation, through the use of composite-based isolators such as hybrid composites between elastomers and metals. However, the interfacial bonding of elastomers and metals still deteriorates under thermo-mechanical stresses.[286] Subtle interfacial failures degrade aerospace isolators, regardless of whether they are passive elastomers or MEAs (MREs, QZS systems, and DEAs). The further development of elastomer chemistry, protective coatings, and the optimization of bonding are required to maintain the high reliability of aerospace systems.

Oil and Gas Industry

Extreme coupled stressors such as high hydrostatic pressure, exposure to seawater, harsh hydrocarbons, and high temperatures are already present in elastomer–metal interfaces in offshore and subsea oil and gas systems, and, because the interfaces are also a critical reliability and safety risk, interfacial degradation becomes an important concern. In underwater connectors, O-rings, and gaskets, adhesion loss, wear, and chemical aging may result in a catastrophic failure of seals with dire consequences in their operations and environment. Although optimization of mechanical design can enhance the initial sealing performance, e.g., sustaining contact pressures above 361 MPa to have leak-free operation under bending loads,[287] long-term durability is often constrained by the wear of the elastomer–metal interface. Experiments on hydrothermal aging of silicone rubber and epoxy and high-performance polymers reveal significant erosion of mechanical and dielectric properties in combined heat and moisture environments,[288] whereas reliability tests of electrical submersible pump tubing–hanger connectors point to erosion of elastomer oxidation, embrittlement, and incompatibility of fluids as the leading failure modes in high-pressure/high-temperature environments.[289]

The interfacial longevity is additionally regulated by the compatibility of materials with fuels and process fluids. The most-used elastomers in sealing applications, such as EPDM, FKM, LSR, ACM, and HNBR, have had their modulus, glass temperature, swelling, and tensile properties drastically altered in acidic, alkaline or biofuel-rich environments, which directly undermines the adhesion and sealing properties.[290–292] The quantification of these effects is carried out using immersion and tensile testing, which is done systematically. Elastomer-based O-rings as depicted in Fig. 8 are subjected to hook-mounted fixtures in a universal testing machine to avoid the surface damage during the loading process, so that the tensile strength and elongation of the O-rings after exposing them to fuel can be accurately measured by standardized procedures.[295] It was found that swelling-induced softening and loss of strength are sensitive indicators of fuel compatibility and interfacial degradation which are revealed by such testing. In response to these difficulties, materials engineering processes have tended toward the development of multifunctional elastomer systems, such as composite gaskets,

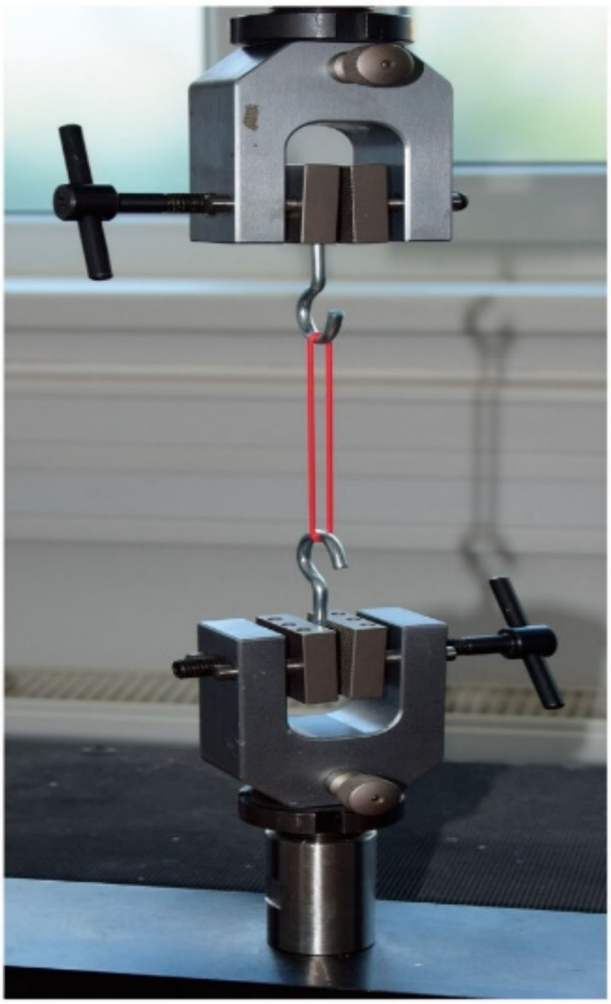

Fig. 8. Tensile testing setup for elastomer O-rings using hook fixtures to prevent surface damage, enabling evaluation of mechanical integrity and fuel compatibility under oil and gas service conditions. Reproduced from Ref. 295 under the Creative Commons CC BY 4.0 license.

carbon-filled silicone interfaces, sensor-integrated (HM-enabled) seals that integrate mechanical resilience with real-time health monitoring.[293,294] In general, the combination of optimized contact mechanics and chemically compatible elastomer formulations, strong elastomer–metal adhesion, and predictive degradation monitoring under realistic service conditions is what is needed to produce reliable oil and gas sealing systems in the long run.

Medical Devices with Elastomer–Metal Interfaces

The incorporation of elastomer–metal interfaces into healthcare equipment is of paramount importance in terms of stability, serviceability, and patient safety, and this complexity is susceptible to corrosion, wear, and adhesion failures. Flexible wearable sensors are examples of cyclic loading. A CNT-coated porous elastomer sponge was capable of stable sensing between 10 Pa and 1.2 MPa under bending to enable gait and tactile monitoring,[296] whereas micro-porous dielectric elastomers provided reliable piezocapacitive sensing.[297] Limited to fatigue, ingress of moisture, and interfacial degradation, biomedical metals' adhesion is enhanced using surface modification techniques. Stainless-steel 316L oxidation in a plasma environment elevated surface energy (83.19 mN m^{-1}) and enhanced silicone rubber adhesion (0.12–0.89 MPa), suppressing delamination and corrosion effects.[298] Compared to that, GaInSn liquid metals exhibit unstable adhesion, because of the variable oxide skins, leading to the unpredictable performance against physiological stresses.[299] Hybrid systems, such as biopolymer-based, e.g., bacterial cellulose reinforced with PDMS hosting printed metal precursors, can create stretchable transistors but are inherently unstable to high temperatures, solvents, and UV radiation.[300]

Hydrogen-bonding supramolecular elastomer healing can be small cracks, in which case the heal speeds up, scaling with the length of the cracks and the inverse height of the healing energy barrier.[301] Analogously, PDMS-based thermoelectric generators can deliver energy harvesting, yet are subject to fatigue when exposed to thermal cycling and body fluid exposure.[302] Elastomeric biomaterials are also at risk of biofouling, and bacterial, protein, and lipid protein attachment to zwitterionic sulfobetaine silane (SBSi) coatings are inhibited, retaining bioinertness throughout 30 days, and preventing biofilm-mediated corrosion.[303] In the meantime, the possibility of tissue engineering with elastomeric biomaterials, such as thermoplastic rubbers and elastic proteins or elastomer–ceramic composites, continues to lag behind the natural tissues in terms of resistance to biodegradation and fluid penetration.[304] Generally, biomedical elastomer–metal interfaces are extremely vulnerable to interfacial wear and tear in the form of fatigue, delamination, and biofouling, as described in Table V. Use of advancements in surface engineering, self-healing elastomers, and antifouling coatings lies in the future to make the devices last longer in clinical settings.

FUTURE OUTLOOK AND RESEARCH GAP

The potential application of hybrid interfaces and multi-material systems have been gaining momentum due to multi-functionality, long life, and sustainability, but they tend to become fraught with interfacial degradation, such as corrosion, wear, and adhesion failures, particularly in elastomer–metal combinations exposed to cyclic and harsh environments. Elastomer–metal core–shell-based liquid metal lattice materials offer shape-memory, programmed rigidity, and energy absorption, but exhibit interfacial instability and corrosion, which reduce reliability. Extrusion-based additive fabrication becomes a problem as there is poor adhesion at

Table V. Environmental degradation and reliability challenges in medical devices with elastomer–metal interfaces

Application	Materials	Degradation	Mechanisms	References
Hybrid elastomer–metal–biopolymer systems	Bacterial cellulose + PDMS with printed metal precursors	Heat, solvent, and UV-induced degradation	Preserved stretchability and microfibril architecture for biomedical devices, but limited long-term stability	14
Flexible and wearable sensors	CNT-coated porous elastomer sponge	Mechanical fatigue, bending stresses	Stable electromechanical response across 10–1.2 MPa range; applicable to gait and tactile monitoring	296
Piezocapacitive tactile sensors	Microporous dielectric elastomers	Moisture ingress and structural fatigue	Reliable sensing via deformation-driven capacitance changes	297
Surface modification for adhesion	Stainless-steel 316L + silicone rubber	Weak adhesion, interfacial corrosion	Plasma oxidation increased surface energy (83.19 mN m^{-1}) and pull-off adhesion (0.12 $\rightarrow$ 0.89 MPa)	298
Liquid metal elastomer systems	GaInSn alloys	Oxide layer, adhesion variability	Strong adhesion when oxide ruptured, weak when intact; performance inconsistent under physiological stress	299, 300
Self-healing elastomer networks	Supramolecular hydrogen-bonding polymers	Crack propagation, delamination	Autonomous self-repair under cyclic loading; improved durability of flexible devices	301
Flexible thermoelectric generators	PDMS composites for biosensors	Interfacial fatigue, thermal cycling	Provided energy harvesting for wearables; susceptible to long-term degradation in fluids	302
Biofouling-resistant coatings	Zwitterionic SBSi-modified elastomers	Biofilm formation, corrosion	Maintained superhydrophilicity and bioinertness for 30 days; suppressed bacterial/protein adhesion	303
Tissue engineering biomaterials	Thermoplastic rubbers, elastic proteins, elastomer–ceramic composites	Biodegradation, fluid infiltration	Mechanical compliance achieved, but resilience lower than natural tissues	304

the polymer–polymer and polymer–metal joints which cause premature failures, and interface optimization is necessary to prevent moisture-based delamination and stress corrosion. Similarly, 3D lithography-based and electrodeposition-fabricated metal–polymer hybrid microstructures can be used to perform microrobots but delaminate during repeated actuation, whereas DIW-printed ceramic–metal–elastomers have bonding and durability issues.

Hybrid laminates like FMLs and elastomer–interlayer types (HyCEMLs, FMELs) will enhance damping and help reduce thermal mismatch stress, but still fail by adhesion under high humidity, cycling, and corrosive environments. Wearable electronics also emphasize weak points: hydrogel–thermochromic elastomer yarns and hydrogel–elastomer TENG systems demonstrate excellent functionality but are susceptible to hydrolysis, peeling, and the chemical incompatibility of the elastomer and metal. Hybrids that focus on sustainability combine recyclability and self-healing, such as elastomer–silica vitrimers, natural rubber–silica composites and nano-chitosan-reinforced styrene–butadiene rubbers. Because of the beneficial properties of elastomers, bioinspired strategies are being actively used to increase the wear resistance, corrosion protection, and adhesive resistance of the elastomer–metal interface. Mussel-inspired chemistry is a process that integrates ferric ions into rubber networks with high oxygen content to form metal–oxygen coordination cross-links and exploits them as sacrificial bonds to enhance strength, toughness, and damping, and to improve shape-memory so that they can withstand more damage under varying stresses. This is further enhanced by sacrificial bonding that is prevalent in natural load-bearing structures, hence increasing reliability.

Sacrificial units are covalently and non-covalently embedded in elastomers/nanocomposites to sequential dissipation of energy to overcome crack initiation and extend adhesive performance under cyclic loading, corrosion, and wear. Skin-based nanostructured elastomer–cellulose composites mimic nonlinear elasticity, providing resilience to repeated deformation serpentine-structured deterministic composites, which reduce stress concentrations at elastomer–metal junctions by distributing the strain. Nanopatterning of elastomer surfaces, such as by nanodimpling, leads to bio-inspired surfaces which increase adhesion and reduce friction through the dissipation of pull-off energy, benefitting interfacial stability in corrosive and abrasive environments. Hierarchical systems also hold

promise: carbon nanodots in diene–rubber networks exhibit a combination of physical/chemical crosslinks and hydrogen bonding, and give sequential paths of dissipation and high toughness. Butadiene–styrene–vinylpyridine rubbers with sacrificial metal–ligand functions have also been shown to enhance modulus, toughness, and resistance to thermal degradation, avoiding adhesion degradation under excursions in the environment. Musculoskeletal models have sparked the development of flexible dielectric elastomer actuators which simulate actuation to an elbow joint and impose stresses more homogeneously, making them less prone to crack formation and debonding under repeated applied stresses.

CONCLUSION

Environmental, chemical, mechanical, and electrochemical stressors interact as couples to control the degree of degradation of elastomer–metal interfaces instead of acting independently. It has always been demonstrated in the literature that moisture, temperature cycling, oxidative conditions, and mechanical loading are synergistically effective at increasing corrosion, wear, and loss of adhesion in chemically-assisted aging of elastomers, electrochemical metal degradation, and mechanically-driven crack initiation and propagation. Surface treatments, coupling agents, multifunctional fillers, and nanostructured or bio-inspired architectures, have greatly contributed to interfacial durability. Adaptive methods with dynamic bonding, sacrificial networks, and self-healing methods will show improved fatigue, wear, and environmental-assisted delamination resistance copmared with standard, similarly static, adhesive or barrier techniques. Current models typically do not represent the distributed damage, wear-based degradation, or chemo-mechanical evolution with time. Scalability limits, complexity of processing, and long-term stability are also limitations that restrict the industrial use of self-healing and bio-based systems. Comprehensively, long-term elastomer–metal interfaces need multifunctional and adaptive designs with explicit consideration of coupled chemo-mechanical and electrochemical processes. Combinations of advanced material strategies and multiscale experimental characterization and predictive modeling will offer a route to enhanced reliability, sustainability, and performance in challenging engineering process conditions.

FUNDING

Not Applicable.

DATA AVAILABILITY

The data utilized is confidential.

CONFLICT OF INTEREST

The authors declare they have no conflicts of interest.

ETHICAL APPROVAL

Not Applicable.

REFERENCES

1. I.R. Sare, J.I. Mardel, and A.J. Hill, *Wear* 250, 1 https://doi.org/10.1016/S0043-1648(01)00622-6 (2001).
2. W. Balasooriya, B. Schrittesser, G. Pinter, and T. Schwarz, *Polym. Test.* 69, 107 https://doi.org/10.1016/j.polymertesting.2018.05.016 (2018).
3. C. Lu, S. Xu, D. Tang, J. Wang, S. Gao, C. Wang, Q. Yong, and F. Chu, *J. Colloid Interface Sci.* 700, 138605 https://doi.org/10.1016/j.jcis.2025.138605 (2025).
4. A. Vohra, K. Schlingman, R.S. Carmichael, and T.B. Carmichael, *Chem* 4, 1673 https://doi.org/10.1016/j.chempr.2018.04.019 (2018).
5. F. Sun, J. Zhang, T. Liu, H. Yao, L. Wang, H. Meng, and J. Fu, *Adv. Mater.* 36(50), 2410650 https://doi.org/10.1002/adma.202410650 (2024).
6. H. Kim, R.-U. Kim, K.-H. Chung, J.-H. An, H.-G. Jeon, and B.-J. Kim, *Polym. Test.* 40, 13 https://doi.org/10.1016/j.polymertesting.2014.08.004 (2014).
7. Z. Shen, R. Dong, J. Li, Y. Su, and X. Long, *J. Manuf. Process.* 109, 359 https://doi.org/10.1016/j.jmapro.2023.10.030 (2024).
8. C. Pan, E.J. Markvicka, M.H. Malakooti, J. Yan, L. Hu, K. Matyjaszewski, and C. Majidi, *Adv. Mater.* 31, 1900663 https://doi.org/10.1002/adma.201900663 (2019).
9. S. Hoshian, V. Jokinen, and S. Franssila, *Soft Matter* 12, 6526 https://doi.org/10.1039/C6SM01095D (2016).
10. M. Hussain, Y.H. Ko, and Y.H. Choa, *J. Nanomater.* 2016, 1 https://doi.org/10.1155/2016/8515103 (2016).
11. M.R. Kibbe, J. Martinez, D.A. Popowich, M.R. Kapadia, S.S. Ahanchi, O.O. Aalami, Q. Jiang, A.R. Webb, J. Yang, T. Carroll, and G.A. Ameer, *J. Biomed. Mater. Res.* 93A, 314 https://doi.org/10.1002/jbm.a.32537 (2010).
12. A. Padsalgikar, E. Cosgriff-Hernandez, G. Gallagher, T. Touchet, C. Iacob, L. Mellin, A. Norlin-Weissenrieder, and J. Runt, *J. Biomed. Mater. Res.* 103, 159 https://doi.org/10.1002/jbm.b.33161 (2015).
13. C. Lv, J. Wang, Z. Li, K. Zhao, and J. Zheng, *Compos. Part B Eng.* 177, 107270 https://doi.org/10.1016/j.compositesb.2019.107270 (2019).
14. I. You, M. Kong, and U. Jeong, *Acc. Chem. Res.* 52, 63 https://doi.org/10.1021/acs.accounts.8b00488 (2019).
15. V. Ghazanfari, A. Taheri, Y. Amini, and F. Mansourzade, *Case Stud. Therm. Eng.* 53, 103864 https://doi.org/10.1016/j.csite.2023.103864 (2024).
16. D. He, Z. Wang, X. Zeng, J. Fan, L. Ren, G. Du, R. Sun, and X. Zeng, *ACS Appl. Mater. Interfaces* 14, 33912 https://doi.org/10.1021/acsami.2c09761 (2022).
17. J. Fan, J. Huang, M. Yan, Z. Gong, L. Cao, and Y. Chen, *J. Mater. Chem. A* 8, 16376 https://doi.org/10.1039/D0TA05725H (2020).
18. T.L. Sun, F. Luo, W. Hong, K. Cui, Y. Huang, H.J. Zhang, D.R. King, T. Kurokawa, T. Nakajima, and J.P. Gong, *Macromolecules* 50, 2923 https://doi.org/10.1021/acs.macromol.7b00162 (2017).
19. X. Zou, K. Chen, H. Yao, C. Chen, X. Lu, P. Ding, M. Wang, X. Hua, and A. Shan, *ACS Appl. Mater. Interfaces* 14, 27383 https://doi.org/10.1021/acsami.2c04971 (2022).
20. L. Sandrin and E. Sacher, *Appl. Surf. Sci.* 135, 339 https://doi.org/10.1016/S0169-4332(98)00302-X (1998).
21. M. Gensch, M. Schwartzkopf, C.J. Brett, S.J. Schaper, L.P. Kreuzer, N. Li, W. Chen, S. Liang, J. Drewes, O. Polonskyi, T. Strunskus, F. Faupel, P. Müller-Buschbaum, and S.V.

Roth, *ACS Appl. Nano Mater.* 4, 4245 https://doi.org/10.1021/acsanm.1c00829 (2021).
22. A.V. Vázquez, A.P. Boughton, N.E. Shephard, S.M. Rhodes, and Z. Chen, *ACS Appl. Mater. Interfaces* 2, 96 https://doi.org/10.1021/am900612r (2010).
23. C. Li, B. Wang, L. Zhou, X. Hou, and S. Su, *SILICON* 14, 10495 https://doi.org/10.1007/s12633-022-01748-x (2022).
24. L. Picard, P. Phalip, E. Fleury, and F. Ganachaud, *Prog. Org. Coat.* 87, 250 https://doi.org/10.1016/j.porgcoat.2015.02.022 (2015).
25. L. Picard, P. Phalip, E. Fleury, and F. Ganachaud, *Prog. Org. Coat.* 80, 120 https://doi.org/10.1016/j.porgcoat.2014.11.022 (2015).
26. L.A. Bloomfield, *Int. J. Adhes. Adhes.* 68, 239 https://doi.org/10.1016/j.ijadhadh.2016.04.001 (2016).
27. D. Ahn, N.E. Shephard, P.A. Olney, and C.S. McMillan, *Macromolecules* 40, 3904 https://doi.org/10.1021/ma070615h (2007).
28. D. Presto, J. Meyerhofer, G. Kippenbrock, S. Narayanan, J. Ilavsky, S. Moctezuma, M. Sutton, and M.D. Foster, *ACS Appl. Mater. Interfaces* 12, 47891 https://doi.org/10.1021/acsami.0c12106 (2020).
29. F. Ehrburger-Dolle, I. Morfin, F. Bley, F. Livet, G. Heinrich, Y. Chushkin, and M. Sutton, *Soft Matter* 15, 3796 https://doi.org/10.1039/C8SM02289E (2019).
30. W. Chen, H. Qiao, D. Zhang, X. Tian, and L. Jin, *Iran. Polym. J.* 32, 715 https://doi.org/10.1007/s13726-023-01152-1 (2023).
31. Y. Chen, Z. He, H. Li, D. Lu, Y. Song, L. Zhan, and W. Liu, *Chin. J. Aeronaut.* https://doi.org/10.1016/j.cja.2025.103496 (2025).
32. Z. Wang, L. Ren, X. Zeng, W. Ye, Y. Xu, X. Zeng, Y. Pang, and S. Rong, The study of effects on the thermo-mechanical performance of the first level thermal interface materials. In 2021 22nd International conference on electronic packaging technology (ICEPT), IEEE, Xiamen, China, 1–6 2021 https://doi.org/10.1109/ICEPT52650.2021.9567919.
33. K. Koh, H. Hwang, C. Park, J.Y. Lee, T.Y. Jeon, S.-H. Kim, J.K. Kim, and U. Jeong, *ACS Appl. Mater. Interfaces* 8, 28149 https://doi.org/10.1021/acsami.6b08270 (2016).
34. N.N. Khanh and K.B. Yoon, *J. Am. Chem. Soc.* 131, 14228 https://doi.org/10.1021/ja905534k (2009).
35. X. Qiu, H. Yin, Q. Xing, and Q. Jin, *Polymers* 15, 2746 https://doi.org/10.3390/polym15122746 (2023).
36. V. Prakash, N. Subasree, V. Arul, M.S. Kumar, P. Dharani, K. Radhakrishnan, and J.V. Kumar, *JOM*. https://doi.org/10.1007/s11837-026-08133-8 (2026).
37. W. Han, H.-P. Zhang, X. Xu, and Y. Tang, *Compos. Part A Appl. Sci. Manuf.* 112, 283 https://doi.org/10.1016/j.compositesa.2018.06.019 (2018).
38. G. Cai, H. Wang, D. Jiang, and Z. Dong, *Prog. Org. Coat.* 123, 337 https://doi.org/10.1016/j.porgcoat.2018.07.025 (2018).
39. Y. Li, H. Jin, S. Nie, C. Tong, and N. Gao, *AIP Adv.* 8, 015313 https://doi.org/10.1063/1.5012097 (2018).
40. C. Cong, C. Cui, X. Meng, S. Lu, and Q. Zhou, *Chem. Res. Chin. Univ.* 29, 806 https://doi.org/10.1007/s40242-013-2401-7 (2013).
41. X. Long, R. Dong, J. Li, Y. Su, C. Chang, F. Jia, and X. Wan, *Int. J. Solids Struct.* 312, 113285 https://doi.org/10.1016/j.ijsolstr.2025.113285 (2025).
42. K. Efimenko, W.E. Wallace, and J. Genzer, *J. Colloid Interface Sci.* 254, 306 https://doi.org/10.1006/jcis.2002.8594 (2002).
43. M. Cai, S. Nie, Y. Du, C. Wang, and J. Song, *ACS Appl. Mater. Interfaces* 11, 14340 https://doi.org/10.1021/acsami.9b01551 (2019).
44. J. Tracy, D.R. D'hooge, N. Bosco, C. Delgado, and R. Dauskardt, *Prog. Photovolt* 26, 981 https://doi.org/10.1002/pip.3045 (2018).
45. Y. Berdichevsky, J. Khandurina, A. Guttman, and Y.-H. Lo, *Sens. Actuators B Chem.* 97, 402 https://doi.org/10.1016/j.snb.2003.09.022 (2004).
46. W.R. Childs, M.J. Motala, K.J. Lee, and R.G. Nuzzo, *Langmuir* 21, 10096 https://doi.org/10.1021/la050011b (2005).
47. F. Cheng, S.-G. Hong, and C.-A. Ho, *J. Adhes.* 67, 123 https://doi.org/10.1080/00218469808011103 (1998).
48. K. Fujimoto, Y. Takebayashi, H. Inoue, and Y. Ikada, *J. Polym. Sci. A Polym. Chem.* 31, 1035 https://doi.org/10.1002/pola.1993.080310426 (1993).
49. S. Dasgupta, *J. Appl. Polym. Sci.* 41, 233 https://doi.org/10.1002/app.1990.070410119 (1990).
50. S. Oprea and V. Oprea, *Eur. Polym. J.* 38, 1205 https://doi.org/10.1016/S0014-3057(01)00280-4 (2002).
51. M.A.F. Johari, I. Aznam, S.A. Mazlan, U. Ubaidillah, N.A. Nordin, S.M. Yusuf, N.H. Lazim, and S.A.A. Aziz, *Results Eng.* 24, 103610 https://doi.org/10.1016/j.rineng.2024.103610 (2024).
52. I.U. Vakarelski, A. Toritani, M. Nakayama, and K. Higashitani, *Langmuir* 17, 4739 https://doi.org/10.1021/la001588q (2001).
53. G.A. Willing, T.H. Ibrahim, F.M. Etzler, and R.D. Neuman, *J. Colloid Interface Sci.* 226, 185 https://doi.org/10.1006/jcis.2000.6801 (2000).
54. E. Porte, S. Eristoff, A. Agrawala, and R. Kramer-Bottiglio, *Soft Robot.* 11, 118 https://doi.org/10.1089/soro.2023.0004 (2024).
55. V. Khuu, M. Osterman, A. Bar-Cohen, and M. Pecht, *IEEE Trans. Device Mater. Relib.* 9, 379 https://doi.org/10.1109/TDMR.2009.2025367 (2009).
56. B. Putz, B. Völker, C. Semprimoschnig, and M.J. Cordill, *Microelectron. Eng.* 167, 17 https://doi.org/10.1016/j.mee.2016.10.012 (2017).
57. Z. Zhang and T. Li, *Scr. Mater.* 59, 862 https://doi.org/10.1016/j.scriptamat.2008.06.058 (2008).
58. N.E. Jansson, Y. Leterrier, and J.-A.E. Månson, *Eng. Fract. Mech.* 73, 2614 https://doi.org/10.1016/j.engfracmech.2006.04.013 (2006).
59. P. Galvez, S. De Lopez Armentia, J. Abenojar, and M.A. Martinez, *Compos. Struct.* 247, 112443 https://doi.org/10.1016/j.compstruct.2020.112443 (2020).
60. R.-Y. Wang, Z.-F. Dou, H.-S. Li, N. Li, X.-R. Liu, and W.-F. Zhang, *Polymer* 328, 128398 https://doi.org/10.1016/j.polymer.2025.128398 (2025).
61. Y. Gao, S. Li, S. He, X. Gu, Y. Yue, Y. Chen, H. Zou, Z. Xing, and Q. Liu, *Prog. Org. Coat.* 192, 108503 https://doi.org/10.1016/j.porgcoat.2024.108503 (2024).
62. K. Sabbagh, R. Kessentini, O. Klinkova, I. Tawfiq, and C. Bouraoui, *Int. J. Mech. Sci.* 303, 110618 https://doi.org/10.1016/j.ijmecsci.2025.110618 (2025).
63. B. Fasolt, F. Welsch, M. Jank, and S. Seelecke, *Smart Mater. Struct.* 28, 094002 https://doi.org/10.1088/1361-665X/ab2f34 (2019).
64. R.E. Whittaker, *Polymer* 13, 169 https://doi.org/10.1016/0032-3861(72)90041-9 (1972).
65. J. Zhang, X. Shi, H. Lu, K. Yu, and Y.-Q. Fu, *Macromolecules* 55, 10320 https://doi.org/10.1021/acs.macromol.2c01423 (2022).
66. H.J. Lim, G. Kim, and G.J. Yun, *ACS Appl. Mater. Interfaces* 15, 24257 https://doi.org/10.1021/acsami.2c15451 (2023).
67. U. Kulshrestha, T. Gupta, P. Kumawat, H. Jaiswal, S.B. Ghosh, and N.N. Sharma, *Polym. Test.* 90, 106676 https://doi.org/10.1016/j.polymertesting.2020.106676 (2020).
68. P. Liu, Y. Wang, H. Hao, S. Basu, X. Feng, Y. Xu, J.A. Boscoboinik, J. Nanda, J. Watt, and D. Mitlin, *Adv. Mater.* 32, 2002908 https://doi.org/10.1002/adma.202002908 (2020).
69. Y. Liu, X. Xu, O.O. Kapitanova, P.V. Evdokimov, Z. Song, A. Matic, and S. Xiong, *Adv. Energy Mater.* 12, 2103589 https://doi.org/10.1002/aenm.202103589 (2022).
70. Q. Meng, *Mech. Mater.* 148, 103516 https://doi.org/10.1016/j.mechmat.2020.103516 (2020).
71. M. Ganser, F.E. Hildebrand, M. Kamlah, and R.M. McMeeking, *J. Mech. Phys. Solids* 125, 681 https://doi.org/10.1016/j.jmps.2019.01.004 (2019).

72. Z. Zhang, F. Guo, Y. Ke, C. Xiang, and X. Jia, *Mater. Des.* 224, 111314 https://doi.org/10.1016/j.matdes.2022.111314 (2022).
73. A. Wineman, *Mech. Res. Commun.* 94, 28 https://doi.org/10.1016/j.mechrescom.2018.08.012 (2018).
74. S. Zhang, L. Han, H. Bai, C. Li, X. Wang, Z. Yang, M. Zai, H. Ma, and Y. Li, *ACS Sustain. Chem. Eng.* 9, 8053 https://doi.org/10.1021/acssuschemeng.1c02319 (2021).
75. A. Mlyniec, A. Morawska-Chochol, K. Kloch, and T. Uhl, *Polym. Degrad. Stab.* 99, 290 https://doi.org/10.1016/j.polymdegradstab.2013.10.018 (2014).
76. M. Patel and A.R. Skinner, *Polym. Degrad. Stab.* 73, 399 https://doi.org/10.1016/S0141-3910(01)00118-5 (2001).
77. M. Johlitz and A. Lion, *Continuum Mech. Thermodyn.* 25, 605 https://doi.org/10.1007/s00161-012-0255-8 (2013).
78. A. Cruz, *Solid State Ionics* 159, 301 https://doi.org/10.1016/S0167-2738(03)00034-1 (2003).
79. Z. Ju, X. Tao, Y. Wang, Q. Yang, T. Liu, J. Nai, W. Zhang, S. Chen, Y. Liu, H. Tian, and J. Lu, *Energy Environ. Sci.* 17, 4703 https://doi.org/10.1039/D4EE01359J (2024).
80. H. Lin, D. Zheng, X. Wu, R. He, L. He, X. Zhou, H. Zuo, C. Yuan, B. Zeng, Y. Xu, and L. Dai, *Sci. Adv.* 10, eadp0730 https://doi.org/10.1126/sciadv.adp0730 (2024).
81. Y. Wu, D. Zhang, Y. Zhang, H. Zhang, L. Zhou, Y. Liu, W. Liu, and Z. Ding, *Nano Energy* 142, 111207 https://doi.org/10.1016/j.nanoen.2025.111207 (2025).
82. H. Zhang, Y. Guo, H. Xu, G. Zhao, and B. Yang, *Chem. Lett.* 50, 844 https://doi.org/10.1246/cl.210019 (2021).
83. X. Liu, X. Xu, F. Zhang, X. Ge, H. Ji, Y. Li, S. Lu, and Z. Wen, *J. Mater. Chem. A* 10, 18616 https://doi.org/10.1039/D2TA05071D (2022).
84. J. Ma, X. Pang, Z. Chen, L. Du, and P. Qiu, *Appl. Mater. Today* 44, 102682 https://doi.org/10.1016/j.apmt.2025.102682 (2025).
85. F. Ciucci and C. Chen, *Electrochim. Acta* 167, 439 https://doi.org/10.1016/j.electacta.2015.03.123 (2015).
86. M.B. Effat and F. Ciucci, *Electrochim. Acta* 247, 1117 https://doi.org/10.1016/j.electacta.2017.07.050 (2017).
87. H. Touzi, Y. Chevalier, R. Kalfat, and N. Jaffrezic-Renault, *Eur. Polym. J.* 56, 140 https://doi.org/10.1016/j.eurpolymj.2014.04.010 (2014).
88. N. Yang, H. Meng, D. Guo, Y. Song, Y. Shi, J. Niu, and F. Wang, *Adv. Sci.* 12, e06640 https://doi.org/10.1002/advs.202506640 (2025).
89. J. Han, K. Lu, Y. Yue, C. Mei, C. Huang, Q. Wu, and X. Xu, *Ind. Crops Prod.* 128, 94 https://doi.org/10.1016/j.indcrop.2018.11.004 (2019).
90. D. Nguyen Dang, B. Peraudeau, S. Cohendoz, S. Mallarino, X. Feaugas, and S. Touzain, *Electrochim. Acta* 124, 80 https://doi.org/10.1016/j.electacta.2013.08.111 (2014).
91. Z. Wang, C. Yin, J. Li, Y. Yang, L. Chen, Y. Luo, Y. Liu, C. He, and P. Fang, *J. Mater. Sci.* 53, 12871 https://doi.org/10.1007/s10853-018-2523-x (2018).
92. Y. Gao, J. Wang, X. Liang, Z. Yan, Y. Liu, and Y. Cai, *IEEE Trans. Dielectr. Electr. Insul.* 21, 2428 https://doi.org/10.1109/TDEI.2014.004476 (2014).
93. Z. Wang, L.H. Zhao, Z.D. Jia, and Z.C. Guan, *IEEE Trans. Dielectr. Electr. Insul.* 24, 2440 https://doi.org/10.1109/TDEI.2017.006610 (2017).
94. K.L. Dagnon, K. Shanmuganathan, C. Weder, and S.J. Rowan, *Macromolecules* 45, 4707 https://doi.org/10.1021/ma300463y (2012).
95. P.K. Annamalai, K.L. Dagnon, S. Monemian, E.J. Foster, S.J. Rowan, and C. Weder, *ACS Appl. Mater. Interfaces* 6, 967 https://doi.org/10.1021/am404382x (2014).
96. Z. Wang, Z.D. Jia, M.H. Fang, and Z.C. Guan, *IEEE Trans. Dielectr. Electr. Insul.* 22, 3357 https://doi.org/10.1109/TDEI.2015.005192 (2015).
97. M. Liu, I.A. Kinloch, R.J. Young, and D.G. Papageorgiou, *Compos. Part B Eng.* 178, 107506 https://doi.org/10.1016/j.compositesb.2019.107506 (2019).
98. G. Ramorino, F. Bignotti, S. Pandini, and T. Riccò, *Compos. Sci. Technol.* 69, 1206 https://doi.org/10.1016/j.compscitech.2009.02.023 (2009).
99. K. Nawaz, U. Khan, N. Ul-Haq, P. May, A. O'Neill, and J.N. Coleman, *Carbon* 50, 4489 https://doi.org/10.1016/j.carbon.2012.05.029 (2012).
100. A. Novikov, J. Goding, C. Chapman, E. Cuttaz, and R.A. Green, *APL Mater.* 8, 101105 https://doi.org/10.1063/5.0005410 (2020).
101. J. Wang, X. Guo, and D. Wu, *J. Polym. Eng.* 40, 57 https://doi.org/10.1515/polyeng-2019-0276 (2019).
102. C.H. Chan and H.W. Kammer, *J. Appl. Polym. Sci.* 110, 424 https://doi.org/10.1002/app.28555 (2008).
103. F. Alloin, A. D'Aprea, N.E. Kissi, A. Dufresne, and F. Bossard, *Electrochim. Acta* 55, 5186 https://doi.org/10.1016/j.electacta.2010.04.034 (2010).
104. A.C.-Y. Ko, A. Burnett, L. Chen, and K. Liu, Galvanic corrosion mechanism and suppressed solution on Al/Cu pads. In 2015 IEEE 22nd International symposium on the physical and failure analysis of integrated circuits, IEEE, Hsinchu, 259–262 2015 https://doi.org/10.1109/IPFA.2015.7224391.
105. Y.J. Kim, I. Bumadian, and J.-S. Park, *J. Mater. Civ. Eng.* 28, 04015129 https://doi.org/10.1061/(ASCE)MT.1943-5533.0001405 (2016).
106. L. Gonzalezprieto, P. Sorichetti, and S. Romano, *Int. J. Hydrogen Energy* 33, 3531 https://doi.org/10.1016/j.ijhydene.2007.10.036 (2008).
107. M.M. Maru, M.M. Lucchese, C. Legnani, W.G. Quirino, A. Balbo, I.B. Aranha, L.T. Costa, C. Vilani, L.A. De Sena, J.C. Damasceno, T. Dos Santos Cruz, L.R. Lidízio, R. E Ferreira Silva, A. Jorio, and C.A. Achete, *Fuel Process. Technol.* 90, 1175 https://doi.org/10.1016/j.fuproc.2009.05.014 (2009).
108. W.V. Liebig, V. Sessner, K.A. Weidenmann, and L. Kärger, *Compos. Struct.* 202, 1109 https://doi.org/10.1016/j.compstruct.2018.05.051 (2018).
109. S. Roth, M. Stoll, K.A. Weidenmann, S. Coutandin, and J. Fleischer, *Int. J. Adv. Manuf. Technol.* 104, 1293 https://doi.org/10.1007/s00170-019-04103-4 (2019).
110. M. Stoll, F. Stemmer, S. Ilinzeer, and K.A. Weidenmann, *KEM* 742, 287 https://doi.org/10.4028/www.scientific.net/KEM.742.287 (2017).
111. A. Hahn, S. Günther, P. Wagener, and S. Barcikowski, *J. Mater. Chem.* 21, 10287 https://doi.org/10.1039/c0jm04480f (2011).
112. K. House, F. Sernetz, D. Dymock, J.R. Sandy, and A.J. Ireland, *Am. J. Orthod. Dentofacial Orthop.* 133, 584 https://doi.org/10.1016/j.ajodo.2007.03.021 (2008).
113. S. Zhang, J.S. Andre, L. Hsu, A. Toolis, S.L. Esarey, B. Li, and Z. Chen, *Macromolecules* 53, 10189 https://doi.org/10.1021/acs.macromol.0c01862 (2020).
114. C. Zhang, J.N. Myers, and Z. Chen, *Langmuir* 30, 12541 https://doi.org/10.1021/la502239u (2014).
115. E.R. Duranty, T.J. Roosendaal, S.G. Pitman, J.C. Tucker, S.L. Owsley, J.D. Suter, and K.J. Alvine, *Rev. Sci. Instrum.* 88, 095114 https://doi.org/10.1063/1.5001836 (2017).
116. C. Kenel, P. Schloth, S. Van Petegem, J.L. Fife, D. Grolimund, A. Menzel, H. Van Swygenhoven, and C. Leinenbach, *JOM* 68, 978 https://doi.org/10.1007/s11837-015-1774-0 (2016).
117. A. Deschamps, L. Lae, and P. Guyot, *Acta Mater.* 55, 2775 https://doi.org/10.1016/j.actamat.2006.12.015 (2007).
118. X. Li, F. Tian, P. Zhou, C. Yang, X. Li, F. Bian, and J. Wang, *RSC Adv.* 6, 81552 https://doi.org/10.1039/C6RA17671B (2016).
119. D.J. Tobler and L.G. Benning, *Geochim. Cosmochim. Acta* 114, 156 https://doi.org/10.1016/j.gca.2013.03.045 (2013).
120. J. Yang, B.D. Siempelkamp, D. Liu, and T.L. Kelly, *ACS Nano* 9, 1955 https://doi.org/10.1021/nn506864k (2015).
121. C. Xiao, Z. Li, H. Guthrey, J. Moseley, Y. Yang, S. Wozny, H. Moutinho, B. To, J.J. Berry, B. Gorman, Y. Yan, K. Zhu, and M. Al-Jassim, *J. Phys. Chem. C* 119, 26904 https://doi.org/10.1021/acs.jpcc.5b09698 (2015).
122. Z. Wang, H. Lin, Y. Wang, X. Yin, J. Li, and Y. Wang, *Langmuir*. https://doi.org/10.1021/acs.langmuir.5c03249 (2025).

123. C. Putignano, J. Le Rouzic, T. Reddyhoff, G. Carbone, and D. Dini, *Proc. Inst. Mech. Eng. J. Eng. Tribol.* 228, 1112 https://doi.org/10.1177/1350650114530681 (2014).
124. B.N.J. Persson, *Matter* 18, 789 https://doi.org/10.1088/0953-8984/18/32/025 (2006).
125. B. Pinedo, M. Hadfield, I. Tzanakis, M. Conte, and M. Anand, *Tribol. Int.* 127, 24 https://doi.org/10.1016/j.triboint.2018.05.032 (2018).
126. X. Tian and F.E. Kennedy, *J. Tribol.* 115, 411 https://doi.org/10.1115/1.2921652 (1993).
127. X. Tian and F.E. Kennedy, *J. Tribol.* 116, 167 https://doi.org/10.1115/1.2927035 (1994).
128. H. Ashrafizadeh, P. Mertiny, and A. McDonald, *Wear* 368–369, 26 https://doi.org/10.1016/j.wear.2016.08.008 (2016).
129. L. Yu, S. Vudayagiri, L.A. Jensen, and A.L. Skov, *Int. J. Smart Nano Mater.* 11, 129 https://doi.org/10.1080/19475411.2020.1768605 (2020).
130. M. Mofidi and B. Prakash, *Tribol. Mater. Surf. Interfaces* 4, 26 https://doi.org/10.1179/175158310X481745 (2010).
131. B.N.J. Persson, U. Tartaglino, O. Albohr, and E. Tosatti, *Nat. Mater.* 3, 882 https://doi.org/10.1038/nmat1255 (2004).
132. S. Xiao, K.A. Laux, H. Wang, F. Hu, and H.-J. Sue, *Wear* 418–419, 281 https://doi.org/10.1016/j.wear.2018.10.009 (2019).
133. H. Rajashekaraiah, S. Bheemappa, S.-H. Yang, and S. Mohan, *Int. J. Precis. Eng. Manuf.* 17, 755 https://doi.org/10.1007/s12541-016-0093-x (2016).
134. C.L. Johnson and A.C. Dunn, *Wear* 438–439, 203066 https://doi.org/10.1016/j.wear.2019.203066 (2019).
135. M.-X. Shen, F. Dong, Z.-X. Zhang, X.-K. Meng, and X.-D. Peng, *Tribol. Int.* 103, 1 https://doi.org/10.1016/j.triboint.2016.06.025 (2016).
136. J.W. Jeong, S.R. Yang, Y.H. Hur, S.W. Kim, K.M. Baek, S. Yim, H.-I. Jang, J.H. Park, S.Y. Lee, C.-O. Park, and Y.S. Jung, *Nat. Commun.* 5, 5387 https://doi.org/10.1038/ncomms6387 (2014).
137. B. Winkeljann, P.A. Leipold, and O. Lieleg, *Adv. Mater. Interfaces* 6, 1900366 https://doi.org/10.1002/admi.201900366 (2019).
138. J. Wang, F. Yan, and Q. Xue, *Wear* 267, 1634 https://doi.org/10.1016/j.wear.2009.06.015 (2009).
139. H. Hirani and M. Verma, *Tribol. Int.* 42, 378 https://doi.org/10.1016/j.triboint.2008.07.014 (2009).
140. J. Yuan, L. Wang, C. Wang, G. Dong, J. Wang, Y. Li, and W. Xu, *Arch. Civ. Mech. Eng.* 25(5), 277 https://doi.org/10.1007/s43452-025-01333-0 (2025).
141. B.A. Obadele, A. Andrews, M.B. Shongwe, and P.A. Olubambi, *Mater. Chem. Phys.* 171, 239 https://doi.org/10.1016/j.matchemphys.2016.01.013 (2016).
142. A. Ayyagari, C. Barthelemy, B. Gwalani, R. Banerjee, T.W. Scharf, and S. Mukherjee, *Mater. Chem. Phys.* 210, 162 https://doi.org/10.1016/j.matchemphys.2017.07.031 (2018).
143. S. Atashin, M. Pakshir, and A. Yazdani, *Mater. Des.* 32, 1315 https://doi.org/10.1016/j.matdes.2010.09.024 (2011).
144. N. Nemati, M. Bozorg, O.V. Penkov, D.-G. Shin, A. Sadighzadeh, and D.-E. Kim, *ACS Appl. Mater. Interfaces* 9, 30149 https://doi.org/10.1021/acsami.7b08565 (2017).
145. X.-Q. Zheng and Y. Liu, *Int. J. Refract. Met. Hard Mater.* 78, 193 https://doi.org/10.1016/j.ijrmhm.2018.09.017 (2019).
146. M.R. Thakare, J.A. Wharton, R.J.K. Wood, and C. Menger, *Wear* 263, 125 https://doi.org/10.1016/j.wear.2006.12.047 (2007).
147. R. Aparicio-Fernández, H. Springer, A. Szczepaniak, H. Zhang, and D. Raabe, *Acta Mater.* 107, 38 https://doi.org/10.1016/j.actamat.2016.01.048 (2016).
148. B.-X. Hou, H.-H. Sheu, M.-Y. Lin, C.-Y. Lee, and H.-B. Lee, *Coatings* 15, 649 https://doi.org/10.3390/coatings15060649 (2025).
149. F.D. Novoa, D.C. Miller, and R.H. Dauskardt, *Sol. Energy Mater. Sol. Cells* 120, 87 https://doi.org/10.1016/j.solmat.2013.08.020 (2014).
150. F.D. Novoa, D.C. Miller, and R.H. Dauskardt, *Prog. Photovolt: Res. Appl.* 24, 183 https://doi.org/10.1002/pip.2657 (2016).
151. P. Sánchez-Friera, M. Piliougine, J. Peláez, J. Carretero, and M. De Sidrach Cardona, *Prog. Photovoltaics.* 19, 658 https://doi.org/10.1002/pip.1083 (2011).
152. A. Kamer, K. Larson-Smith, L.S.C. Pingree, and R.H. Dauskardt, *Thin Solid Films* 519, 1907 https://doi.org/10.1016/j.tsf.2010.08.116 (2011).
153. R.B. Malla, M.R. Shrestha, M.T. Shaw, and S.B. Brijmohan, *J. Mater. Civ. Eng.* 23, 287 https://doi.org/10.1061/(ASCE)MT.1943-5533.0000166 (2011).
154. B. Golaz, V. Michaud, and J.-A.E. Månson, *Int. J. Adhes. Adhes.* 31, 805 https://doi.org/10.1016/j.ijadhadh.2011.07.009 (2011).
155. Y. Gao, C. Li, J. Wang, B. Wang, and X. Cui, *Polym. Degrad. Stab.* 169, 108989 https://doi.org/10.1016/j.polymdegradstab.2019.108989 (2019).
156. A. Manikkavel, V. Kumar, and D.-J. Lee, *Theor. Appl. Fract. Mech.* 108, 102626 https://doi.org/10.1016/j.tafmec.2020.102626 (2020).
157. H. Yuk, T. Zhang, G.A. Parada, X. Liu, and X. Zhao, *Nat. Commun.* 7, 12028 https://doi.org/10.1038/ncomms12028 (2016).
158. A. Valenza, V. Fiore, and L. Fratini, *Int. J. Adv. Manuf. Technol.* 53, 593 https://doi.org/10.1007/s00170-010-2866-1 (2011).
159. L. Liao and C. Huang, *Int. J. Adhes. Adhes.* 68, 389 https://doi.org/10.1016/j.ijadhadh.2015.12.013 (2016).
160. M. Jung Lee, T. Min Cho, W. Seock Kim, B. Chai Lee, and J. Ju Lee, *Int. J. Adhes. Adhes.* 30, 322 https://doi.org/10.1016/j.ijadhadh.2009.10.005 (2010).
161. H. Wang, J. Wang, and J. Chen, *Eng. Fract. Mech.* 132, 104 https://doi.org/10.1016/j.engfracmech.2014.10.029 (2014).
162. G. Stamoulis, N. Carrere, J.Y. Cognard, P. Davies, and C. Badulescu, *Int. J. Adhes. Adhes.* 51, 148 https://doi.org/10.1016/j.ijadhadh.2014.03.002 (2014).
163. P. Weißgraeber and W. Becker, *Int. J. Solids Struct.* 50, 2383 https://doi.org/10.1016/j.ijsolstr.2013.03.012 (2013).
164. I.S. Floros, K.I. Tserpes, and T. Löbel, *Compos. Part B Eng.* 78, 459 https://doi.org/10.1016/j.compositesb.2015.04.006 (2015).
165. I. Katsivalis, O.T. Thomsen, S. Feih, and M. Achintha, *Int. J. Adhes. Adhes.* 97, 102479 https://doi.org/10.1016/j.ijadhadh.2019.102479 (2020).
166. A.V.M. Rocha, A. Akhavan-Safar, R. Carbas, E.A.S. Marques, R. Goyal, M. El-zein, and L.F.M. Da Silva, *Theoret. Appl. Fract. Mech.* 106, 102493 https://doi.org/10.1016/j.tafmec.2020.102493 (2020).
167. L. Zhao, Y. Gong, J. Zhang, Y. Chen, and B. Fei, *Compos. Struct.* 116, 509 https://doi.org/10.1016/j.compstruct.2014.05.042 (2014).
168. J.C.S. Azevedo, R.D.S.G. Campilho, F.J.G. Da Silva, T.M.S. Faneco, and R.M. Lopes, *Theoret. Appl. Fract. Mech.* 80, 143 https://doi.org/10.1016/j.tafmec.2015.09.007 (2015).
169. H.-C. Zhang, B. Kang, L.-S. Chen, and X. Lu, *Polym. Test.* 87, 106521 https://doi.org/10.1016/j.polymertesting.2020.106521 (2020).
170. S. Pan, F. Zhang, P. Cai, M. Wang, K. He, Y. Luo, Z. Li, G. Chen, S. Ji, Z. Liu, X.J. Loh, and X. Chen, *Adv. Funct. Mater.* 30, 1909540 https://doi.org/10.1002/adfm.201909540 (2020).
171. H. Xu, Y. Zhang, J. Yang, L. Ye, Q. Wu, B. Qu, Q. Wang, and Z. Wang, *Polym. Chem.* 4, 3028 https://doi.org/10.1039/c3py00185g (2013).
172. M. Sankarasubramanian, M. Torabizadeh, Z.A. Putnam, J.C. Moosbrugger, M.Y. Huang, and S. Krishnan, *Polym. Test.* 78, 105932 https://doi.org/10.1016/j.polymertesting.2019.105932 (2019).
173. P.K. Chattopadhyay, N.C. Das, and S. Chattopadhyay, *Compos. Part A Appl. Sci. Manuf.* 42, 1049 https://doi.org/10.1016/j.compositesa.2011.04.011 (2011).

174. M. Shang, Y. Wu, B. Shentu, and Z. Weng, *Ind. Eng. Chem. Res.* 58, 12650 https://doi.org/10.1021/acs.iecr.9b00691 (2019).
175. A. Naeim Abadi, H. Garmabi, and F. Hemmati, *Adv. Polym. Technol.* 37, 2303 https://doi.org/10.1002/adv.21906 (2018).
176. W. Wang, X. Ma, D. Sun, X. Qi, J. Yang, and Y. Wang, *Compos. Part A Appl. Sci. Manuf.* 128, 105671 https://doi.org/10.1016/j.compositesa.2019.105671 (2020).
177. A.M. Grande, S.J. Garcia, and S. Van Der Zwaag, *Polymer* 56, 435 https://doi.org/10.1016/j.polymer.2014.11.052 (2015).
178. S. Fu, B. Yu, L. Duan, H. Bai, F. Chen, K. Wang, H. Deng, Q. Zhang, and Q. Fu, *Compos. Sci. Technol.* 108, 23 https://doi.org/10.1016/j.compscitech.2015.01.001 (2015).
179. H. Bai, D. Bai, H. Xiu, H. Liu, Q. Zhang, K. Wang, H. Deng, F. Chen, Q. Fu, and F.-C. Chiu, *RSC Adv.* 4, 49374 https://doi.org/10.1039/C4RA08823A (2014).
180. H. Liu, H. Bai, D. Bai, Z. Liu, Q. Zhang, and Q. Fu, *Polymer* 108, 38 https://doi.org/10.1016/j.polymer.2016.11.034 (2017).
181. K. Tian, Z. Suo, and J.J. Vlassak, *ACS Appl. Mater. Interfaces* 12, 31002 https://doi.org/10.1021/acsami.0c07468 (2020).
182. S.S. Banerjee, K.D. Kumar, A.K. Sikder, and A.K. Bhowmick, *Macro Chem. Phys.* 216, 1666 https://doi.org/10.1002/macp.201500173 (2015).
183. R. Akhtar, N. Schwarzer, M.J. Sherratt, R.E.B. Watson, H.K. Graham, A.W. Trafford, P.M. Mummery, and B. Derby, *J. Mater. Res.* 24, 638 https://doi.org/10.1557/jmr.2009.0130 (2009).
184. Z. Wei, G. Zhang, H. Chen, J. Luo, R. Liu, and S. Guo, *J. Mater. Res.* 24, 801 https://doi.org/10.1557/jmr.2009.0126 (2009).
185. C.A. Charitidis, *Ind. Eng. Chem. Res.* 50, 565 https://doi.org/10.1021/ie100099g (2011).
186. P.V. Kolluru, M.D. Eaton, D.W. Collinson, X. Cheng, D.E. Delgado, K.R. Shull, and L.C. Brinson, *Macromolecules* 51, 8964 https://doi.org/10.1021/acs.macromol.8b01426 (2018).
187. P. Schön, S. Dutta, M. Shirazi, J. Noordermeer, and G. Julius Vancso, *J. Mater. Sci.* 46, 3507 https://doi.org/10.1007/s10853-011-5259-4 (2011).
188. L. Morales-Rivas, A. González-Orive, C. Garcia-Mateo, A. Hernández-Creus, F.G. Caballero, and L. Vázquez, *Sci. Rep.* 5, 17164 https://doi.org/10.1038/srep17164 (2015).
189. F. Crippa, P.-A. Thorén, D. Forchheimer, R. Borgani, B. Rothen-Rutishauser, A. Petri-Fink, and D.B. Haviland, *Soft Matter* 14, 3998 https://doi.org/10.1039/C8SM00149A (2018).
190. S. Wijesinghe, D. Perahia, and G.S. Grest, *Macromolecules* 51, 7621 https://doi.org/10.1021/acs.macromol.8b01449 (2018).
191. Z. Zeng and J.-C. Tan, *ACS Appl. Mater. Interfaces* 9, 39839 https://doi.org/10.1021/acsami.7b13402 (2017).
192. H. Ade and A.P. Hitchcock, *Polymer* 49, 643 https://doi.org/10.1016/j.polymer.2007.10.030 (2008).
193. A. Yudhanto and G. Lubineau, X-ray computed tomography for assessing impact damage in composites. In Non-destructive testing of impact damage in fiber-reinforced polymer composites, Elsevier, 187–213 2024 https://doi.org/10.1016/B978-0-443-14120-1.00007-8.
194. M.J. Blunt, B. Bijeljic, H. Dong, O. Gharbi, S. Iglauer, P. Mostaghimi, A. Paluszny, and C. Pentland, *Adv. Water Resour.* 51, 197 https://doi.org/10.1016/j.advwatres.2012.03.003 (2013).
195. M.L. Cummings, T.Y. Chien, C. Preissner, V. Madhavan, D. Diesing, M. Bode, J.W. Freeland, and V. Rose, *Ultramicroscopy* 112, 22 https://doi.org/10.1016/j.ultramic.2011.09.018 (2012).
196. T. Sui, E. Salvati, H. Zhang, I.P. Dolbnya, and A.M. Korsunsky, *Mater. Today Adv.* 4, 100024 https://doi.org/10.1016/j.mtadv.2019.100024 (2019).
197. L. Song, D. Liu, H. Zhang, Y. Wang, B. Zhao, W. Kang, Y. Zhu, Y. Wei, and Y. Song, *Nano Lett.* 25, 2618 https://doi.org/10.1021/acs.nanolett.4c04547 (2025).
198. L. Cristofolini, *Curr. Opin. Colloid Interface Sci.* 19, 228 https://doi.org/10.1016/j.cocis.2014.03.006 (2014).
199. Q. Gan, L. Song, Y. Wang, Q. Yuan, W. Huang, Y. Zhu, Y. Huang, and Y. Song, *Nano Energy* 120, 109141 https://doi.org/10.1016/j.nanoen.2023.109141 (2024).
200. G. Hu, D. Bonanno, Y. Su, X. Zhao, Y. Krishnamachari, W. Forrest, S. Persak, J. Givand, D. Mannes, M. Olbinado, M. Wagner, C. Grünzweig, and V. Novak, *Pharm. Res.* 41, 547 https://doi.org/10.1007/s11095-024-03673-7 (2024).
201. P. Cloetens, R. Barrett, J. Baruchel, J.-P. Guigay, and M. Schlenker, *J. Phys. D Appl. Phys.* 29, 133 https://doi.org/10.1088/0022-3727/29/1/023 (1996).
202. X. Hu, L. Wang, F. Xu, T. Xiao, and Z. Zhang, *Carbon* 67, 368 https://doi.org/10.1016/j.carbon.2013.10.007 (2014).
203. Y. Jing and P. Huang, *Comput. Mater. Sci.* 177, 109574 https://doi.org/10.1016/j.commatsci.2020.109574 (2020).
204. K. Ghosh and B. Shrimali, *Finite Elem. Anal. Des.* 247, 104348 https://doi.org/10.1016/j.finel.2025.104348 (2025).
205. D. Lu, F. Meng, X. Zhou, Y. Zhuo, Z. Gao, and X. Du, *J. Eng. Mech.* 149(12), 4023102 https://doi.org/10.1061/JENMDT.EMENG-7206 (2023).
206. L.B. Hu, Y. Cong, Z.X. Xia, S.T. Gu, and Z.-Q. Feng, *Eng. Fract. Mech.* 310, 110444 https://doi.org/10.1016/j.engfracmech.2024.110444 (2024).
207. Z. Zhang, X. Men, Y. Pan, Z. Wang, Q. Shi, and X. Fu, *Mater. Today Commun.* 32, 103848 https://doi.org/10.1016/j.mtcomm.2022.103848 (2022).
208. S.J. Yang, S.I. Rosenbloom, B.P. Fors, and M.N. Silberstein, *Mech. Mater.* 188, 104863 https://doi.org/10.1016/j.mechmat.2023.104863 (2024).
209. H. Moslemzadeh and S. Mohammadi, *Int. J. Solids Struct.* 256, 111983 https://doi.org/10.1016/j.ijsolstr.2022.111983 (2022).
210. J. Chen, F. Wang, G. Shi, G. Cao, Y. He, W. Ge, H. Liu, and H. Wu, *J. Pet. Sci. Eng.* 125, 146 https://doi.org/10.1016/j.petrol.2014.11.011 (2015).
211. Y. Masrar and M. Ettaouil, *Appl. Math. Comput.* 404, 126218 https://doi.org/10.1016/j.amc.2021.126218 (2021).
212. M. Wang and X. Hang, *Materials* 16, 1345 https://doi.org/10.3390/ma16041345 (2023).
213. Z. Liao, W. Wei, L. Zhang, Y. Gao, and Y. Cai, *Comput. Ind.* 168, 104285 https://doi.org/10.1016/j.compind.2025.104285 (2025).
214. F. Tao, Q. Qi, L. Wang, and A.Y.C. Nee, *Engineering* 5, 653 https://doi.org/10.1016/j.eng.2019.01.014 (2019).
215. L. Jin, X. Zhai, K. Wang, K. Zhang, D. Wu, A. Nazir, J. Jiang, and W.-H. Liao, *Mater. Des.* 244, 113086 https://doi.org/10.1016/j.matdes.2024.113086 (2024).
216. Y. Pang, T. He, S. Liu, X. Zhu, and C. Lee, *Adv. Sci.* 11, 2306574 https://doi.org/10.1002/advs.202306574 (2024).
217. M.-H. Nguyen, A. Onken, A. Wulff, K. Foremny, P. Torgau, H. Schütte, S. Hild, and T. Doll, *Bioengineering* 10, 625 https://doi.org/10.3390/bioengineering10050625 (2023).
218. Y. Zhao, J. Jing, L. Chen, F. Xu, and H. Hou, *Acta Metall. Sin.* 57(9), 1107 https://doi.org/10.11900/0412.1961.2021.00051 (2021).
219. E.V. Shilko, A.I. Dmitriev, R.R. Balokhonov, and V.A. Romanova, *Phys. Mesomech.* 27, 493 https://doi.org/10.1134/S1029959924050011 (2024).
220. S.R. Kalidindi, M. Buzzy, B.L. Boyce, and R. Dingreville, *Front. Mater.* 9, 818535 https://doi.org/10.3389/fmats.2022.818535 (2022).
221. Y. Martinez, L. Rojas, A. Peña, M. Valenzuela, and J. Garcia, *Mathematics* 13, 1571 https://doi.org/10.3390/math13101571 (2025).
222. Z. Zhang, L. Wang, and C. Lee, *Adv. Sens. Res.* 2, 2200072 https://doi.org/10.1002/adsr.202200072 (2023).
223. A. Grard, L. Belec, and F.X. Perrin, *Prog. Org. Coat.* 140, 105513 https://doi.org/10.1016/j.porgcoat.2019.105513 (2020).

224. A. Grard, L. Belec, and F.X. Perrin, *Int. J. Adhes. Adhes.* 102, 102656 https://doi.org/10.1016/j.ijadhadh.2020.102656 (2020).
225. J.-I. Moon, Y.-H. Lee, H.-J. Kim, S.-M. Noh, and J.-H. Nam, *Prog. Org. Coat.* 75, 65 https://doi.org/10.1016/j.porgcoat.2012.03.009 (2012).
226. T. Pössinger, C. Bolzmacher, L. Bodelot, and N. Triantafyllidis, *Microsyst. Technol.* 20, 803 https://doi.org/10.1007/s00542-013-2036-0 (2014).
227. B. Golaz, V. Michaud, and J.-A.E. Månson, *Compos. Part A Appl. Sci. Manuf.* 48, 171 https://doi.org/10.1016/j.compositesa.2013.01.017 (2013).
228. K.-B. Sim, D. Baek, J.-H. Shin, G.-S. Shim, S.-W. Jang, H.-J. Kim, J.-W. Hwang, and J.U. Roh, *Polymers* 12, 556 https://doi.org/10.3390/polym12030556 (2020).
229. N. Encinas, J. Abenojar, and M.A. Martínez, *Int. J. Adhes. Adhes.* 33, 1 https://doi.org/10.1016/j.ijadhadh.2011.10.002 (2012).
230. N. Encinas, B. Díaz-Benito, J. Abenojar, and M.A. Martínez, *Surf. Coat. Technol.* 205, 396 https://doi.org/10.1016/j.surfcoat.2010.06.069 (2010).
231. N. Encinas, M. Pantoja, J. Abenojar, and M.A. Martínez, *J. Adhes. Sci. Technol.* 24, 1869 https://doi.org/10.1163/016942410X511042 (2010).
232. T.S. Williams, H. Yu, and R.F. Hicks, *J. Adhes. Sci. Technol.* 28, 653 https://doi.org/10.1080/01694243.2013.859646 (2014).
233. E. Squiller, K. Danielmeier, and P. Kruppa, Polyurethanes: coatings, adhesives and sealants, Vincentz Network, Hannover, Germany, 2019 https://doi.org/10.1515/9783748600473.
234. D.H. Kim, W. Lee, J.B. Park, and J.U. Lee, *Micromachines* 16, 399 https://doi.org/10.3390/mi16040399 (2025).
235. Y. Lin, X. Dong, S. Liu, S. Chen, Y. Wei, and L. Liu, *ACS Appl. Mater. Interfaces* 8, 24143 https://doi.org/10.1021/acsami.6b08587 (2016).
236. I.O. Arukalam, E.E. Oguzie, and Y. Li, *J. Colloid Interface Sci.* 512, 674 https://doi.org/10.1016/j.jcis.2017.10.089 (2018).
237. E.R. Sadiku, A. Babul Reddy, D. Gnanasekarana, B. Oboirien, B.A. Aderibigbe, K. Varaprasad, and S.M.R. Goddeti, Nanostructured polymer blends for gas/vapor barrier and dielectric applications. In Design and applications of nanostructured polymer blends and nanocomposite systems, Elsevier, 239–259 2016 https://doi.org/10.1016/B978-0-323-39408-6.00011-X.
238. I. Saarikoski, F. Joki-Korpela, M. Suvanto, T.T. Pakkanen, and T.A. Pakkanen, *Surf. Sci.* 606, 91 https://doi.org/10.1016/j.susc.2011.09.005 (2012).
239. J. Wang, Y. Liu, Y. Zhang, J. Feng, H. Wang, Y. Yu, and H. Sun, *Adv. Funct. Mater.* 28, 1800625 https://doi.org/10.1002/adfm.201800625 (2018).
240. Z. Sang, K. Ke, and I. Manas-Zloczower, *ACS Appl. Polym. Mater.* 1, 714 https://doi.org/10.1021/acsapm.8b00241 (2019).
241. S.C. Boothroyd, D.W. Johnson, M.P. Weir, C.D. Reynolds, J.M. Hart, A.J. Smith, N. Clarke, R.L. Thompson, and K.S. Coleman, *Chem. Mater.* 30, 1524 https://doi.org/10.1021/acs.chemmater.7b04343 (2018).
242. J. Park, S. Yoon, K. Kang, and S. Jeon, *Small* 6, 1981 https://doi.org/10.1002/smll.201000275 (2010).
243. C.-F. Lin, Y. Qi, K. Gregorczyk, S.B. Lee, and G.W. Rubloff, *Acc. Chem. Res.* 51, 97 https://doi.org/10.1021/acs.accounts.7b00524 (2018).
244. R. Wang, J. Zhang, H. Kang, and L. Zhang, *Compos. Sci. Technol.* 133, 136 https://doi.org/10.1016/j.compscitech.2016.07.019 (2016).
245. S. Qi, M. Yu, J. Fu, M. Zhu, Y. Xie, and W. Li, *Soft Matter* 14, 8521 https://doi.org/10.1039/C8SM01712C (2018).
246. B. Kussmaul, S. Risse, G. Kofod, R. Waché, M. Wegener, D.N. McCarthy, H. Krüger, and R. Gerhard, *Adv. Funct. Mater.* 21, 4589 https://doi.org/10.1002/adfm.201100884 (2011).
247. B. Zhong, H. Dong, Y. Luo, D. Zhang, Z. Jia, D. Jia, and F. Liu, *Compos. Sci. Technol.* 151, 156 https://doi.org/10.1016/j.compscitech.2017.08.019 (2017).
248. L. Bokobza and C. Belin, *J. Appl. Polym. Sci.* 105, 2054 https://doi.org/10.1002/app.26153 (2007).
249. M. Khalid, A.F. Ismail, C.T. Ratnam, Y. Faridah, W. Rashmi, and M.F. Al Khatib, *Radiat. Phys. Chem.* 79, 1279 https://doi.org/10.1016/j.radphyschem.2010.07.002 (2010).
250. J. Yu, K. Lu, E. Sourty, N. Grossiord, C.E. Koning, and J. Loos, *Carbon* 45, 2897 https://doi.org/10.1016/j.carbon.2007.10.005 (2007).
251. Y. Liu, Z. Tang, Y. Chen, C. Zhang, and B. Guo, *ACS Appl. Mater. Interfaces* 10, 2992 https://doi.org/10.1021/acsami.7b17465 (2018).
252. Y. Chien, W.-T. Chuang, U.-S. Jeng, and S. Hsu, *ACS Appl. Mater. Interfaces* 9, 5419 https://doi.org/10.1021/acsami.6b11993 (2017).
253. D.J. Stuckey, H. Ishii, Q.-Z. Chen, A.R. Boccaccini, U. Hansen, C.A. Carr, J.A. Roether, H. Jawad, D.J. Tyler, N.N. Ali, K. Clarke, and S.E. Harding, *Tissue Eng. Part A* 16, 3395 https://doi.org/10.1089/ten.tea.2010.0213 (2010).
254. Q.-Z. Chen, H. Ishii, G.A. Thouas, A.R. Lyon, J.S. Wright, J.J. Blaker, W. Chrzanowski, A.R. Boccaccini, N.N. Ali, J.C. Knowles, and S.E. Harding, *Biomaterials* 31, 3885 https://doi.org/10.1016/j.biomaterials.2010.01.108 (2010).
255. A. Smejda-Krzewicka, E. Irzmańska, K. Mrozowski, A. Adamus-Włodarczyk, N. Litwicka, K. Strzelec, and M.I. Szynkowska-Jóźwik, *Molecules* 29, 1306 https://doi.org/10.3390/molecules29061306 (2024).
256. L. Wang, Y. Chen, L. Lin, H. Wang, X. Huang, H. Xue, and J. Gao, *Chem. Eng. J.* 362, 89 https://doi.org/10.1016/j.cej.2019.01.014 (2019).
257. A. Artemova, Anti-corrosion carbon-based composite epoxy coating for marine industry, Nanyang Technological University, 2019 https://doi.org/10.32657/10356/142799.
258. Y. Liang, D. Zhang, M. Zhou, Y. Xia, X. Chen, S. Oliver, S. Shi, and L. Lei, *Prog. Org. Coat.* 148, 105844 https://doi.org/10.1016/j.porgcoat.2020.105844 (2020).
259. T. Ghosh and N. Karak, *Prog. Org. Coat.* 139, 105472 https://doi.org/10.1016/j.porgcoat.2019.105472 (2020).
260. L. Mu, Y. Shi, X. Guo, T. Ji, L. Chen, R. Yuan, L. Brisbin, H. Wang, and J. Zhu, *RSC Adv.* 5, 66067 https://doi.org/10.1039/C5RA11093A (2015).
261. S.A. Lawal, I.A. Choudhury, and Y. Nukman, *J. Clean. Prod.* 66, 610 https://doi.org/10.1016/j.jclepro.2013.11.066 (2014).
262. L.V. Rodríguez-de Marcos, J.I. Larruquert, J.A. Méndez, and J.A. Aznárez, *Opt. Mater. Express* 6, 3622 https://doi.org/10.1364/OME.6.003622 (2016).
263. X. Zhang, J. Cao, Y. Yang, X. Wu, Z. Zheng, and X. Zhang, *Chem. Eng. J.* 374, 730 https://doi.org/10.1016/j.cej.2019.05.211 (2019).
264. H. Liang, Y. Li, S. Huang, K. Huang, X. Zeng, Q. Dong, C. Liu, P. Feng, and C. Zhang, *ACS Sustain. Chem. Eng.* 8, 914 https://doi.org/10.1021/acssuschemeng.9b05477 (2020).
265. R.S. Komartin, B. Balanuca, M.I. Necolau, A. Cojocaru, and R. Stan, *Polymers* 13, 3792 https://doi.org/10.3390/polym13213792 (2021).
266. O. Saf, H. Erol, and A.E. Kutlu, *Appl. Acoust.* 165, 107296 https://doi.org/10.1016/j.apacoust.2020.107296 (2020).
267. S. Ahmed, S. Salehi, C. Ezeakacha, and C. Teodoriu, *Polym. Test.* 76, 350 https://doi.org/10.1016/j.polymertesting.2019.03.041 (2019).
268. W. Lou, W. Zhang, T. Jin, X. Liu, and W. Dai, *Polymers* 10, 897 https://doi.org/10.3390/polym10080897 (2018).
269. Z. Wang, C. Chen, Q. Liu, Y. Lou, and Z. Suo, *J. Mech. Phys. Solids* 99, 289 https://doi.org/10.1016/j.jmps.2016.12.007 (2017).
270. E. Ducrot, Y. Chen, M. Bulters, R.P. Sijbesma, and C. Creton, *Science* 344, 186 https://doi.org/10.1126/science.1248494 (2014).
271. J. Yang, A.R. Webb, S.J. Pickerill, G. Hageman, and G.A. Ameer, *Biomaterials* 27, 1889 https://doi.org/10.1016/j.biomaterials.2005.05.106 (2006).

272. T. Grelle, D. Wolff, and M. Jaunich, *Polym. Test.* 48, 44 https://doi.org/10.1016/j.polymertesting.2015.09.009 (2015).
273. M. Jaunich, W. Stark, and D. Wolff, *Polym. Test.* 31, 987 https://doi.org/10.1016/j.polymertesting.2012.07.016 (2012).
274. R.R. Babu, N.K. Singha, and K. Naskar, *Express Polym Lett* 2, 226 https://doi.org/10.3144/expresspolymlett.2008.27 (2008).
275. S.J. Oh and J.L. Koenig, *Rubber Chem. Technol.* 73, 74 https://doi.org/10.5254/1.3547581 (2000).
276. S. Thörmann, M. Markiewicz, and O. Von Estorff, *J. Sound Vib.* 399, 151 https://doi.org/10.1016/j.jsv.2017.03.021 (2017).
277. A. Deaconescu and T. Deaconescu, *Polymers* 17, 1275 https://doi.org/10.3390/polym17091275 (2025).
278. T. Shimizu, S. Nagata, S. Tsuneta, T. Tarbell, C. Edwards, R. Shine, C. Hoffmann, E. Thomas, S. Sour, R. Rehse, O. Ito, Y. Kashiwagi, M. Tabata, K. Kodeki, M. Nagase, K. Matsuzaki, K. Kobayashi, K. Ichimoto, and Y. Suematsu, *Sol. Phys.* 249, 221 https://doi.org/10.1007/s11207-007-9053-z (2008).
279. R. Brancati, G. Di Massa, S. Pagano, and S. Santini, *Meccanica* 54, 333 https://doi.org/10.1007/s11012-019-00951-2 (2019).
280. W. Li, X. Zhang, and H. Du, *J. Intell. Mater. Syst. Struct.* 23, 1041 https://doi.org/10.1177/1045389X11435431 (2012).
281. S. Liu, L. Feng, D. Zhao, X. Shi, Y. Zhang, J. Jiang, Y. Zhao, C. Zhang, and L. Chen, *Smart Mater. Struct.* 28, 085037 https://doi.org/10.1088/1361-665X/ab2e44 (2019).
282. J. Zhou, K. Wang, D. Xu, H. Ouyang, and Y. Fu, *J. Vib. Control* 24, 3278 https://doi.org/10.1177/1077546317703866 (2018).
283. A. Jalali, H. Dianati, M. Norouzi, H. Vatandoost, and M. Ghatee, *J. Intell. Mater. Syst. Struct.* 31, 2002 https://doi.org/10.1177/1045389X20942314 (2020).
284. C. Yang, J. Fu, M. Yu, X. Zheng, and B. Ju, *J. Intell. Mater. Syst. Struct.* 26, 1290 https://doi.org/10.1177/1045389X14541492 (2015).
285. M. Adachi, K. Hamazawa, Y. Mimuro, and H. Kawamoto, *J. Electrostat.* 89, 88 https://doi.org/10.1016/j.elstat.2017.08.003 (2017).
286. K. Ilya, D. Andrey, H. Dmytro, V. Ekaterina, K. Vladislav, and T. Oleg, *Mater. Today Proc.* 30, 393 https://doi.org/10.1016/j.matpr.2019.12.383 (2020).
287. L.-Q. Wang, Z.-L. Wei, S.-M. Yao, Y. Guan, and S.-K. Li, *Chin. J. Mech. Eng.* 31, 18 https://doi.org/10.1186/s10033-018-0209-6 (2018).
288. C. Lesaint, J. Holto, H.H. Saeternes, and M.-H.G. Ese, *IEEE Trans. Dielect. Electr. Insul.* 26, 1139 https://doi.org/10.1109/TDEI.2019.007907 (2019).
289. A. Wilson, *J. Pet. Technol.* 66, 114 https://doi.org/10.2118/0714-0114-JPT (2014).
290. C.-W. Lin, C.-H. Chien, J. Tan, Y.-J. Chao, and J.W. Van Zee, *Int. J. Hydrogen Energy* 36, 6756 https://doi.org/10.1016/j.ijhydene.2011.02.112 (2011).
291. G. Li, J. Tan, and J. Gong, *J. Power. Sources* 205, 244 https://doi.org/10.1016/j.jpowsour.2011.06.092 (2012).
292. Y. Akiyama, H. Sodaye, Y. Shibahara, Y. Honda, S. Tagawa, and S. Nishijima, *J. Power. Sources* 195, 5915 https://doi.org/10.1016/j.jpowsour.2009.11.038 (2010).
293. D. Lee, J.W. Lim, S. Nam, I. Choi, and D.G. Lee, *Compos. Struct.* 128, 284 https://doi.org/10.1016/j.compstruct.2015.03.063 (2015).
294. T. Schotzko, M. Reuter, and W. Lang, *Polym. Test.* 48, 31 https://doi.org/10.1016/j.polymertesting.2015.09.002 (2015).
295. M. Müller, R.K. Mishra, V. Šleger, M. Pexa, and J. Čedík, *Materials* 17, 430 https://doi.org/10.3390/ma17020430 (2024).
296. S. Kim, M. Amjadi, T.-I. Lee, Y. Jeong, D. Kwon, M.S. Kim, K. Kim, T.-S. Kim, Y.S. Oh, and I. Park, *ACS Appl. Mater. Interfaces* 11, 23639 https://doi.org/10.1021/acsami.9b07636 (2019).
297. D. Kwon, T.-I. Lee, J. Shim, S. Ryu, M.S. Kim, S. Kim, T.-S. Kim, and I. Park, *ACS Appl. Mater. Interfaces* 8, 16922 https://doi.org/10.1021/acsami.6b04225 (2016).
298. A. Latifi, M. Imani, M.T. Khorasani, and M. Daliri Joupari, *Appl. Surf. Sci.* 320, 471 https://doi.org/10.1016/j.apsusc.2014.09.084 (2014).
299. K. Doudrick, S. Liu, E.M. Mutunga, K.L. Klein, V. Damle, K.K. Varanasi, and K. Rykaczewski, *Langmuir* 30, 6867 https://doi.org/10.1021/la5012023 (2014).
300. J. Zhu, X. Wang, and Y. Mu, *Comput. Methods Appl. Mech. Eng.* 447, 118355 https://doi.org/10.1016/j.cma.2025.118355 (2025).
301. Y. Chen, A.M. Kushner, G.A. Williams, and Z. Guan, *Nat. Chem.* 4, 467 https://doi.org/10.1038/nchem.1314 (2012).
302. M. Zadan, M.H. Malakooti, and C. Majidi, *ACS Appl. Mater. Interfaces* 12, 17921 https://doi.org/10.1021/acsami.9b19837 (2020).
303. S.-B. Yeh, C.-S. Chen, W.-Y. Chen, and C.-J. Huang, *Langmuir* 30, 11386 https://doi.org/10.1021/la502486e (2014).
304. Q. Chen, S. Liang, and G.A. Thouas, *Prog. Polym. Sci.* 38, 584 https://doi.org/10.1016/j.progpolymsci.2012.05.003 (2013).